

Collimation of astrophysical jets – the rôle of the accretion disk magnetic field distribution

Christian Fendt¹

Max Planck Institute for Astronomy, Königstuhl 17, D-69117 Heidelberg, Germany

fendt@mpia.de

ABSTRACT

We have applied axisymmetric magnetohydrodynamic (MHD) simulations in order to investigate the impact of the accretion disk magnetic flux profile on the collimation of jets. Using the ZEUS-3D code modified for magnetic diffusivity, our simulations evolve from an initial state in hydrostatic equilibrium and a force-free magnetic field configuration. Considering a power law for the disk poloidal magnetic field profile $B_P \sim r^{-\mu}$ and for the density profile of the disk wind $\rho \sim r^{-\mu_\rho}$, we have performed a systematic parameter study over a wide range of parameters μ and μ_ρ . We apply a toy parameterization for the magnetic diffusivity derived from the internal turbulent Alfvénic pressure. We find that the degree of collimation (quantified by the ratio of mass flow rates in axial and lateral direction) decreases for a steeper disk magnetic field profile (increasing μ). Varying the total magnetic flux does not change the degree of jet collimation substantially, it only affects the time scale of outflow evolution and the terminal jet speed. As our major result we find a general relation between the collimation degree with the disk wind magnetization power law exponent. Outflows with high degree of collimation resulting from a flat disk magnetic field profile tend to be unsteady, producing axially propagating knots as discussed earlier in the literature. Depending slightly on the inflow density profile this unsteady behavior sets in for $\mu < 0.4$. We also performed simulations of jet formation with artificially enhanced decay of the toroidal magnetic field component in order to investigate the idea of a purely "poloidal collimation" previously discussed in the literature. These outflows remain only weakly collimated and propagate with lower velocity. Thanks to our large numerical grid size (about 7×14 AU for protostars), we may apply our results to recently observed hints of jet rotation (DG Tau) indicating

¹Part of the numerical work has been accomplished at the Astrophysikalisches Institut Potsdam and at the University of Potsdam, Germany

a relatively flat disk magnetic field profile, $\mu \simeq 0.5$. In general, our results are applicable to both stellar and extragalactic sources of MHD jets.

Subject headings: accretion, accretion disks — MHD — ISM: jets and outflows — stars: mass loss — stars: pre-main sequence — galaxies: jets

1. Introduction

Astrophysical jets as highly collimated high speed beams of matter have been observed as common phenomenon in a variety of astronomical sources, among them young stars, micro-quasars and active galactic nuclei. The current understanding of jet formation is that jets are launched by *magnetohydrodynamic* (MHD) processes in the vicinity of the central jet object – an accretion disk surrounding a protostar or a black hole (Blandford & Payne 1982; Pudritz & Norman 1983; Camenzind 1990). The general properties of jet sources and the ongoing physical processes have been investigated for a long time, however, the principal mechanism which actually *launches* a jet from the disk at a certain time is not yet known.

A number of numerical simulations investigating the MHD jet formation have been published. We may distinguish between those simulations which take into account the evolution of the *disk structure* and those which consider the disk as a fixed *boundary condition* for the simulation of the disk wind. The first approach allows to study directly the launch¹ of the outflow, i.e the ejection of accreting plasma into an outflow in direction vertical to the disk. However, due to the limited time resolution and spatial coverage typical for these simulations, little can be learned concerning the ultimate jet acceleration and collimation which takes place at radii beyond the Alfvén surface (Uchida & Shibata 1985; Miller & Stone 1997; Kudoh et al. 1998). The second approach allows to investigate the *long term evolution* of jet formation on a large spatial scale (Ouyed & Pudritz 1997a,b; Krasnopolsky et al. 1999; Fendt & Elstner 2000; Fendt & Cemeljic 2002). The mechanism which launches the outflow out of the accretion stream cannot be studied by this approach.

In this paper we study how jet formation – i.e. jet collimation and acceleration – depends on the magnetic field profile of the jet launching accretion disk. The initial magnetic field is located in an initially hydrostatic density distribution. We prescribe various magnetic field profiles along the disk surface which is taken as a boundary condition fixed in time. The coronal (i.e. jet) magnetic field evolves in time from the initial state and governed by a

¹By jet *formation* and jet *launching* we denote the acceleration and collimation of a disk wind, and the generation of a disk wind out of the accretion flow, respectively

prescribed mass inflow from the disk surface into the corona. We apply the ZEUS-3D MHD code modified for magnetic diffusivity (Fendt & Cemeljic 2002). It is clear that the "real" disk-jet magnetic field and the mass flux into the jet is a result of dissipative MHD processes in the disk in interaction with the external field structure. The disk structure and evolution will also be affected by the existence of a magnetized disk wind/jet. Although most of the processes involved are understood to some extent, the self-consistent dynamical modeling of such systems has just started (e.g. simulations of a disk dynamo generated jet magnetic field (von Rekowski & Brandenburg 2004)) and the results have to be considered still as preliminary. For the purpose of the present paper we have to keep in mind that some of the parameter runs considered may be more realistic than others concerning the internal disk physics.

We note that in a contemporaneous and independent study Pudritz et al. (2006a) have undertaken a similar approach. Our results generally agree with their paper, but also transcend their approach in several aspects. Among the additional features treated in our paper are a much larger grid, the description of a turbulent magnetic diffusivity, a quantitative measure of the collimation degree, and a broader range of parameters studied.

Our paper is organized as follows. Section 2 briefly summarizes the issue of MHD jet collimation. Section 3 introduces our model approach. In Sect. 4 we present our results before concluding the paper with the summary. Preliminary results of the present investigation have been published earlier (see Fig. 2 in Rüdiger (2002)).

2. Self-collimation of rotating MHD outflows

Theoretical studies considering analytical solutions of the stationary, axisymmetric MHD force-balance in the asymptotic jet flow (i.e. far from the source) have clearly shown that such outflows *must* collimate into a narrow beam when carrying a *net poloidal electric current* (Heyvaerts & Norman 1989; Chiueh et al. 1991). This fundamental statement has been recently confirmed and generalized (Okamoto 2003; Heyvaerts & Norman 2003).

2.1. Stationary studies of MHD jets

A self-consistent treatment of the collimation *process* - i.e. the question how collimation is achieved along the initial outflow - has to consider at least a 2.5-dimensional (i.e. axisymmetric three-dimensional) MHD problem. Until about a decade ago, MHD jet theory has been mostly limited to the stationary approach. Time-independent studies, however,

cannot really prove whether a MHD solution derived will actually be realized during the time evolution of a forming jet. Hence, the final answer concerning jet self-collimation can only be given by time-dependent MHD simulations. Although stationary *self-similar* models gave clear indication for collimated MHD jets (Blandford & Payne 1982; Sauty & Tsinganos 1994; Li 1993; Contopoulos & Lovelace 1994) one has to keep in mind that such a constraint has implications which are critical for collimation, but are not really feasible for jets. For example, self-similarity considers an *infinite jet radius* and does exclude the symmetry axis of the outflow. Truly 2.5-dimensional (axisymmetric 3D) solutions considering the local force-balance and global boundary conditions have been obtained only in the force-free limit (Fendt et al. 1995; Lery et al. 1998; Fendt & Memola 2001), and provide the shape of the collimating jet as determined by the internal force-equilibrium. So far, the only self-consistent two-dimensional stationary MHD solution of a collimating wind flow has been published decades ago (Sakurai 1985, 1987). These solutions collimate on logarithmic scales only - a result of the low rotation rate applied.

2.2. Time-dependent MHD simulations

The first numerical evidence of the MHD jet self-collimation process has been provided by Ouyed & Pudritz (1997a) following a pioneering approach for disk winds by Ustyugova et al. (1995). The simulations by Ouyed & Pudritz were been performed from an initially force-free setup and fixed boundary conditions for the mass inflow into the jet from an underlying Keplerian disk surface. After a few hundred of inner disk rotations the MHD disk wind collimates into a narrow beam and saturates into a stationary state outflow. For a recent review on numerical progress in simulating disk winds and jets we refer to (Pudritz et al. 2006b).

It is clear that different inflow conditions for the disk wind (mass flow rate or magnetic field profile) will result in a different dynamical evolution of the jet, as there are different time scales, velocities or a different degree of collimation. It is therefore interesting to investigate a wide parameter range for the leading jet parameters. This has partly been done in a number of papers discussing the variation of the jet mass load (Ouyed & Pudritz 1999; Kato et al. 2002), a time-dependent disk magnetic field inclination (Krasnopolsky et al. 1999), magnetic diffusivity in the jet (Kuwabara et al. 2000; Fendt & Cemeljic 2002; Kuwabara et al. 2005), time-dependent mass loading (Vitorino et al. 2003), the extension of the simulation box on collimation (Ustyugova et al. 1999), or, in difference to these cases of a monotonously distributed disk magnetic field, the long-term evolution of a stellar dipolar magnetosphere in connection with a Keplerian disk (Fendt & Elstner 2000).

The next step will be to include the disk structure in the numerical simulations (Hayashi et al. 1996; Miller & Stone 1997; Casse & Keppens 2002; Kudoh et al. 2002) and follow the jet launching process over many hundreds of disk rotations. Substantial progress have been made in this respect in simulations already in particular concerning the accretion process from disk down to the star (Romanova et al. 2002, 2003, 2004, 2005) but collimated disk jets have not yet been found.

2.3. “Toroidal or poloidal collimation”?

Concerning jet self-collimation it is interesting to mention a proposal by Spruit et al. (1997) pointing out that the toroidally dominated jet magnetic field is *kink-unstable*. Spruit et al. suggested that jets should be rather collimated by the *poloidal* disk magnetic field pressure and less by the toroidal pinching force. The authors find that “*poloidal collimation*” works best for a disk magnetic field profile $|B_P| \sim r^{-\mu}$ with $\mu \leq 1.3$. Indication for “poloidal collimation” of outflows has been reported also by MHD simulations (Matt et al. 2003), launching the outflow in a dipolar stellar magnetosphere and collimating it by the surrounding disk magnetic field.

The kink instability of jets can be investigated by non-axisymmetric simulations only. It is therefore important to note that 3D-simulations of MHD jet formation have indeed proven the feasibility of MHD self-collimation under the influence of non-axisymmetric perturbations in the jet launching region (Ouyed et al. 2003; Kigure & Shibata 2005). Kelvin-Helmholtz modes are usually fastest growing and are particularly dangerous for the jet in the super-Alfvénic regime. Essentially, it is the “backbone” of the jet flow, i.e. the axial region of high field strength and low density which stabilizes the jet against the instabilities as this highly sub-Alfvénic region of (Ouyed et al. 2003; Pudritz et al. 2006b). In general, the 3D simulations show that the jets starts as a stable outflow, then destabilizes after about 100 inner disk rotations before it stabilizes again at the time of 200 inner disk rotations. The detailed behavior of the different instability modes depend of course on the flow parameters and the general setup of e.g. the non-axisymmetric boundary conditions (see Ouyed et al. (2003) for details).

As an interesting fact, we note that all studies of MHD jet formation so far (time-dependent or stationary) which lead to a collimated jet, the disk magnetic field profile satisfies the Spruit et al. criterion $\mu \leq 1.3$. Examples are the stationary (Blandford & Payne 1982) solution of a self-similar, cold jet with $\mu = 5/4$, simulations of a collimating jet by Ouyed & Pudritz (1997a) applying $\mu = 1$, or by Fendt & Elstner (2000) treating an initially dipolar field distribution $\mu = 3$.

3. Model setup

We perform axisymmetric MHD simulations of jet formation for a set of different boundary conditions for the accretion disk magnetic field. We apply the ZEUS-3D MHD code modified for magnetic diffusivity (Fendt & Cemeljic 2002). As initial state we prescribe a force-free magnetic field within a gas distribution in hydrostatic equilibrium. This is essential in order to avoid artificial relaxation processes caused by a non-equilibrium initial condition. The gas is "cold" and supported by additional turbulent Alfvénic pressure.

A Keplerian disk is taken as a boundary condition for the mass inflow from the disk surface into the corona and the magnetic flux. The poloidal magnetic field lines are anchored in the rotating disk. A gap extends between the central body and the inner disk radius r_1 implying a vanishing mass load for the jet from this region. Compared to our previous studies (Fendt & Elstner 2000; Fendt & Cemeljic 2002), several new features are included in the present approach.

- Our major goal is to investigate a broad parameter range of different accretion disk magnetic flux profiles and disk wind density (i.e. mass flux) profiles.
- We apply a non-equidistant numerical grid covering a large spatial domain of 150×300 inner disk radii corresponding to e.g. about (6.7×13.3) AU assuming an inner disk radius of $10 R_\odot$ for protostars.
- We consider a simple parameterization of turbulent magnetic diffusivity, variable in space and time, in agreement with also considering turbulent Alfvénic pressure. However, compared to our previous studies the magnitude of magnetic diffusivity is low, thus not affecting the degree of jet collimation.

In the following we give some details for the new features of our the model setup.

3.1. Resistive MHD equations

We numerically model the time-dependent evolution of jet formation considering the following set of resistive MHD equations,

$$\frac{\partial \rho}{\partial t} + \nabla \cdot (\rho \vec{v}) = 0, \quad \nabla \cdot \vec{B} = 0, \quad \frac{4\pi}{c} \vec{j} = \nabla \times \vec{B}, \quad (1)$$

$$\rho \left[\frac{\partial \vec{u}}{\partial t} + (\vec{v} \cdot \nabla) \vec{v} \right] + \nabla(p + p_A) + \rho \nabla \Phi - \frac{\vec{j} \times \vec{B}}{c} = 0, \quad (2)$$

$$\frac{\partial \vec{B}}{\partial t} - \nabla \times \left(\vec{v} \times \vec{B} - \frac{4\pi}{c} \eta \vec{j} \right) = 0, \quad (3)$$

$$\rho \left[\frac{\partial e}{\partial t} + (\vec{v} \cdot \nabla) e \right] + p(\nabla \cdot \vec{v}) - \frac{4\pi}{c^2} \eta \vec{j}^2 = 0, \quad (4)$$

with the usual notation for the variables (see Fendt & Elstner (2000)).

We apply a polytropic equation of state for the gas, $p = K \rho^\gamma$ with the polytropic index γ . Thus, we do not solve the energy equation (4) and the internal energy of the gas is reduced ² to $e = p/(\gamma - 1)$. The Ohmic heating term in energy equation (4) has shown to be generally negligible for the dynamics of the system (e.g. Miller & Stone (1997)). This is usually due to the low levels of dissipation presumed in astrophysical cases. Comparison of the compression and dissipation terms shows that this holds also for our study (plasma beta $\beta_i \simeq 1$ and magnetic diffusivity $\eta \simeq 0.01$, see below). On the other hand, simulations treating violent reconnection processes in stellar magnetospheres and/or current sheets have shown that Ohmic heating might establish regions of hot plasma (e.g. Hayashi et al. (1996)). As we are primarily interested in the flow dynamics we neglect Ohmic heating.

Applying a polytropic equation of state simplifies the numerical challenge considerably. We do not believe that this simplification affects the general results of our simulations. Clearly, certain number values numerically derived in our study may well change (as e.g. the exact degree of collimation) and their interpretation must be strictly limited to a comparison *within* our parameter range applied. Future studies on this topic will have to consider and to compare to a non-polytropic equation of state as well. This is, however, beyond the scope of the present paper.

In addition to the hydrostatic gas pressure p we consider *Alfvénic turbulent pressure* assuming $p_A \equiv p/\beta_t$ with $\beta_t = \text{const.}$ This approach has been applied in a series of papers by various groups (Ouyed & Pudritz (1997a), Ouyed & Pudritz (1997b), Fendt & Elstner (2000), Fendt & Cemeljic (2002), Vitorino et al. (2003), Ouyed et al. (2003), Pudritz et al. (2006a)). As we intend to complement these studies, we have followed once again the same approach. In general, turbulent Alfvénic pressure may explain the presence of a *cold* corona above protostellar accretion disks as observationally suggested. We have previously argued that the existence of such an additional pressure component is inevitable as turbulent Alfvén waves will be launched naturally in the highly turbulent accretion disk and then propagate into the disk wind and outflow (Fendt & Cemeljic 2002).

²Note, however, that ongoing work by Clarke and collaborators seems to indicate that relaxation of the polytropy assumption may affect the dynamical evolution in certain domains of the jet, in particular regions with shocks or contact discontinuities (Ramsey & Clarke 2004)

For the polytropic index we apply $\gamma = 5/3$. This is a value generally assumed for non-relativistic astrophysical polytropic gas dynamics. However, note that with such γ , Ohmic heating (see above) and also turbulent Alfvénic pressure is potentially neglected for the thermodynamics. Detailed (linear) analysis of magnetohydrodynamic turbulence in media under various conditions has shown that sub-Alfvénic pressure exerted by Alfvén waves generally obeys a polytropic equation of state with polytropic index $\gamma_t = 1/2$. This has been derived analytically for well defined model assumptions³ which are applicable for a variety of physical states (see McKee & Zweibel (1995)) and has also proven numerically (Gammie & Ostriker 1996; Passot & Vázquez-Semadeni 2003). However, the exact number value of the polytropic index for turbulent Alfvénic pressure in the case of expanding and accelerating magnetohydrodynamic outflows is not known (if it exists at all). Therefore, for simplicity, we apply a turbulent Alfvénic pressure polytropic index equal to that of the gas, $\gamma_t = \gamma = 5/3$. The effective polytropic index for multi-pressure polytropes (N pressure components p_n) would be given by

$$\gamma_{\text{eff}} = \sum_{n=1}^N \left(\frac{p_n}{p} \right) \gamma_n = \frac{\beta_t \gamma + \gamma_t}{\beta_t + 1} \quad (5)$$

(see Curry & McKee (2000) and references therein) indicating that for low β_t the polytrope would be dominated by the turbulent Alfvénic pressure term. For $\gamma_t = \gamma = 5/3$ and $\beta_t \simeq 0.03$, also $\gamma_{\text{eff}} \simeq 5/3$.

We solve the MHD equations applying the ZEUS-3D code (Stone & Norman 1992a,b; Hawley & Stone 1995) in the axisymmetry option for cylindrical coordinates (r, ϕ, z) . We added physical magnetic resistivity to the original ZEUS-3D ideal MHD code (see description and extensive tests in Fendt & Cemeljic (2002)). We normalize all variables to their value measured at the inner disk radius r_i . For example, time is measured in units of the Keplerian period at the inner disk radius, and for the density $\rho \rightarrow \rho/\rho_i$. The point mass for the gravitational potential $\Phi = -1/\sqrt{r^2 + z^2}$ is located at the origin. Finally, the normalized equation of motion treated numerically is

$$\frac{\partial \vec{v}'}{\partial t'} + (\vec{v}' \cdot \nabla') \vec{v}' = \frac{2 \vec{j}' \times \vec{B}'}{\delta_i \beta_i \rho'} - \frac{\nabla'(p' + p'_A)}{\delta_i \rho'} - \nabla' \Phi'. \quad (6)$$

The coefficients $\beta_i \equiv 8\pi p_i/B_i^2$ and $\delta_i \equiv \rho_i v_{K,i}^2/p_i$ with the Keplerian speed $v_{K,i} \equiv (GM/r_i)^{1/2}$, correspond to the plasma beta and the Mach number of the gas at the inner disk radius (Ouyed & Pudritz 1997a). For a “cold” corona with $p'_A > 0$ we have $\beta_t = 1/(\delta_i(\gamma - 1)/\gamma - 1)$.

³A thermodynamic system undergoing temporal changes the *adiabatic* index of (compressible) Alfvén waves is instead $\gamma_{\text{wave}} = 3/2$ (McKee & Zweibel 1995). $P_{\text{wave}} \sim \rho^{1/2}$ applies in steady state media or Alfvén waves propagating in a density gradient.

In the following primes are omitted and only normalized variables are used if not explicitly declared otherwise.

3.2. Turbulent magnetic diffusivity

Magnetic diffusivity caused by turbulent motion in the jet material affects both collimation and acceleration of the jet (Fendt & Cemeljic 2002). Magnetic diffusivity also plays an essential rôle in the jet launching process in the accretion disk (Li 1995; Ferreira 1997). The magnetic diffusivity η we apply in Eq. (3) is “anomalous” and is considered to be provided by macroscopic MHD instabilities. As the jet launching accretion disk is highly turbulent itself, we naturally expect that the turbulent pattern will propagate into the jet when the disk material is lifted up from the disk surface. The turbulence evolution along the jet will certainly be affected by advection and stretching and may vary in different regimes. However, the exact dynamical evolution of turbulence in jets has not yet been investigated and is therefore poorly understood.

Supposing that the magnetic diffusivity is primarily due by the same turbulent Alfvénic waves which are responsible for the turbulent Alfvénic pressure applied in the simulations, we have derived a toy parameterization relating both effects (Fendt & Cemeljic 2002). Such an approach extends and generalizes the studies by Ouyed & Pudritz (1997a), Fendt & Elstner (2000), and Pudritz et al. (2006a). We achieve this by parameterizing the *turbulent magnetic diffusivity* similar to the Shakura-Sunyaev parameterization of turbulent viscosity, $\eta_t = \alpha_m v l$, where $\alpha_m \leq 1$ and l and v are the characteristic dynamical length scale and velocity of the system, respectively.

The turbulent magnetic diffusivity η_t can be related to the Alfvénic turbulent pressure p_A by first selecting the turbulent velocity field v_t (i.e. the *turbulent* Alfvénic velocity) as characteristic velocity. This gives $\eta_t = \alpha_m v_t l$ and with $\beta_t = (c_s/v_t)^2$ and $c_s^2 = \gamma p/\rho$, it follows

$$v_t^2 = \frac{\gamma p}{\beta_t \rho}, \quad \text{or} \quad v_t'^2 = \frac{\gamma}{\delta_i \beta_t} \rho'^{\gamma-1}. \quad (7)$$

For the chosen polytropic index this implies a normalized magnetic diffusivity $\eta \sim \rho^{1/3}$ if l is constant. The power index for $\eta(\rho)$ would be affected by a change in the polytropic index for the turbulent Alfvénic pressure (see discussion above). The characteristic length scale l of turbulent magnetic diffusivity in the jet is not a known quantity. If we assume the turbulence being generated within the disk and launched from there into the outflow, we may assume an initial length scale l corresponding to the Shakura-Sunyaev parameterization of the disk turbulent viscosity, i.e. limited by the disk height $l < h(r)$. In our normalization,

this would imply $l \simeq 0.1$ for regions close to the star as typically $h/r \simeq 0.1$ and $l \simeq 1.0$ at $r \simeq 10$. For regions at greater distance to the star, l could be correspondingly larger. A fully self-consistent treatment of Alfvénic turbulence would have to consider also its temporal and spatial expansion as well as damping or decay as the turbulence cells propagate along the collimating jet. This is clearly beyond the scope of our purpose and we instead *assume* a constant characteristic length scale l .

In our simulations we apply sub-Alfvénic turbulence, $\beta_t = 0.03$ and $\delta_i = 100$ (Ouyed & Pudritz 1997a; Fendt & Cemeljic 2002) resulting in a magnetic diffusivity $\eta = \eta_0 \rho^{1/3}$ with $\eta_0 = 0.03$. This would correspond to a number value $(\alpha_m l) = 0.04$.

We finally note that the magnitude of normalized magnetic diffusivity is in the same range as typically applied in the literature (Hayashi et al. 1996; Miller & Stone 1997; von Rekowski & Brandenburg 2004). In a previous study investigating the relation between magnitude of magnetic diffusivity and degree of jet collimation we have shown that such (low) level of diffusivity does not affect the degree of jet collimation - jet de-collimation as due to magnetic diffusivity applies above a critical diffusivity about a factor of 100 larger as used in the present paper (Fendt & Cemeljic 2002). In fact, as our goal is to study the relation between jet collimation and disk magnetic field distribution, the magnitude of diffusivity was chosen such that it will not affect the degree of collimation.

3.3. Numerical grid

We use the “scaled grid” option by ZEUS with the grid element size decreasing inwards by a factor of 0.99. The numerical grid size is (256×256) resulting in a spatial resolution from (0.13×0.26) close to the origin to (1.6×3.2) at the opposite corner. The physical grid size for all simulations is $(r \times z) = (150 \times 300)r_i$ corresponding to (6.7×13.3) AU for $r_i \simeq 10 R_\odot$ if applied for a protostar. This is several times larger than in previous studies (Ouyed & Pudritz 1997a; Fendt & Cemeljic 2002; Pudritz et al. 2006a) and comparable to the observational resolution for young stars (Bacciotti et al. 2002).

3.4. Initial conditions

Prescribing a stable initial condition is essential for any time-dependent simulation. Otherwise, the early evolution of the system will be dominated by artificial relaxation processes of the instable initial setup. This is particularly important if only few evolutionary time steps are computed.

We start our simulations from a density stratification in hydrostatic equilibrium with an initially force-free (and also current-free) magnetic field. Such a configuration would remain in its initial state if not disturbed by the given boundary conditions. The initial density distribution is $\rho(r, z) = (r^2 + z^2)^{-3/4}$ (Ouyed & Pudritz 1997a; Fendt & Cemeljic 2002).

The initial magnetic field distribution is calculated using a stationary, axisymmetric finite element code described elsewhere (Fendt et al. 1995). Essentially, this code calculates the axisymmetric force-free magnetic flux distribution for *any* given boundary value problem. We compute the ϕ -component of the vector potential⁴ A_ϕ using a numerical grid with twice the resolution of the grid applied in the ZEUS code. Having obtained the vector potential of the initial field distribution by the finite element code, we derive the magnetic field distribution for the time-dependent simulation with respect to the ZEUS-3D *staggered mesh* (see Fendt & Elstner (2000)). Our approach guarantees $|\nabla \cdot \vec{B}| < 10^{-15}$, respectively $|\vec{j} \times \vec{B}| = 0.01|\vec{B}|$.

For the finite element grid, we prescribe the disk magnetic flux $\Psi(r, z = 0) = r^{\mu_\Psi}$ as Dirichlet boundary condition, corresponding to a poloidal magnetic field $B_P(r, 0) \sim r^{-\mu}$ with $\mu = 2 - \mu_\Psi$. Along the axial boundary $\Psi(r = 0, z) = 0$. Along the outer boundaries we prescribe a magnetic flux decreasing towards the axes (here the exact flux profile is marginally important as the initial field will be immediately perturbed by the outflow).

3.5. Boundary conditions

Along the r -boundary we distinguish between the gap region extending from $r = 0$ to $r = r_i = 1.0$ and the disk region from $r = 1.0$ to $r = r_{\text{out}}$. The disk region governs the mass inflow from the disk surface into corona (denoted also as "disk wind" in the following). The poloidal magnetic field along the r -boundary is fixed in time and is, hence, determined by the choice of the initial magnetic flux distribution. Thus, the magnetic flux across the equatorial plane is conserved, $\Psi(r, z = 0; t) = \Psi(r, z = 0; t = 0)$. The poloidal magnetic field profile along the disk is chosen as a power law, $B_P(r, 0) \sim r^{-\mu}$. Equivalent to Ouyed & Pudritz (1997a) the disk toroidal magnetic field component is force free with $B_\phi = \mu_i/r$ for $r \geq r_i$, $\mu_i = B_{\phi,i}/B_i$.

⁴The ϕ -component of the vector potential rA_ϕ is identical to the magnetic flux $\Psi(r, z) = (1/2\pi) \int \vec{B}_P \cdot d\vec{A}$

3.5.1. Hydrodynamic boundary conditions

The hydrodynamic boundary conditions are “inflow” along the r -axis, “reflecting” along the symmetry axis and “outflow” along the outer boundaries. Matter is “injected” from the disk into the corona parallel to the poloidal magnetic field with low velocity $\vec{v}_{\text{inj}}(r, 0) = \nu_i v_K(r) \vec{B}_P / B_P$ and with a density $\rho_{\text{inj}}(r, 0) = \rho_i \rho(r, 0)$. In some simulations we applied a slightly enhanced mass flow rate from the outermost grid elements of the disk by increasing the inflow velocity by a certain factor. This choice helped to deal with some problems at the intersection of inflow and outflow boundary conditions just in the corner at $(r_{\text{max}}, z = 0)$, and does not affect the flow on larger scales. Along the gap, the mass flux into the corona is set to zero. We chose a power law for the inflow density profile,

$$\rho_{\text{inj}}(r, 0) \equiv \rho_0(r) = \rho_i r^{-\mu_\rho}. \quad (8)$$

As a first choice, it is natural to assume $\mu_\rho \sim 3/2$ as this is the disk density profile both for the Shakura-Sunyaev accretion disk and for advection dominated disks (see e.g. the self-similar Blandford & Payne solution, or the Ouyed & Pudritz (1997a) model). This is, however, the average density profile of a thin disk and one may expect deviations from that profile for several reasons. Those may arise (i) as the structure of jet-driving disks can be altered by the outflow, (ii) due to magnetic fields close to equipartition, or may be simply suggested by the fact that (iii) we do not yet fully understand the mass loading of the jet / disk wind out of the accreting matter. We have therefore applied different density profiles $\mu_\rho = 0.3, \dots, 2.0$ for the disk wind mass flux in our simulations.

For the injection velocity, one may assume that the initial disk wind speed is in the range of the sound speed in the disk, $v_{\text{inj}}(r) \simeq c_s(r) \simeq v_{\text{kep}} \sim r^{-1/2}$. However, the actual velocity along the disk surface will be different from the thin disk estimate and will, moreover, depend in detail from the launching mechanism. For simplicity, all simulations presented in the paper assume the same injection velocity. Therefore, the total mass flux profile is varied only by the density profile.

3.5.2. The disk magnetic field profile

The disk magnetic flux profile is less constrained, or better, less understood. A thin disk equipartition magnetic field will follow a profile $\sim r^{-5/4}$ (Blandford & Payne 1982). However, it is not clear to date where the disk/jet magnetic field originates, how it is generated and how it evolves. We find it therefore valuable to explore a wider range of disk magnetic flux profiles. This is the main goal of the present paper. The choice of having a certain disk magnetic field distribution fixed in time should be understood as this field structure being

determined by the internal disk physics (implying that different disk internal conditions may lead to a different disk flux distribution). In this respect, we do not care about how the magnetic field has been *built up* in time. Instead, we assume that internal disk processes like diffusion, advection, or turbulence work together in generating and supporting a large scale stationary field structure with the chosen disk surface field distribution. In the introduction we have already stressed the point that concerning the internal disk physics and the interaction between disk and outflow (in both directions) some of the parameter runs considered may finally be proven to be more realistic than others if compared to a fully self-consistent simulation including the disk internal disk physics and dynamics in relation with the outflow itself. So far, this problem has not been solved in generality, although there are first simulations treating the disk-jet system over many hundreds of rotational periods applying simplified disk models (Casse & Keppens 2002; Kudoh et al. 2002; Cemeljic & Fendt 2004; von Rekowski & Brandenburg 2004). In particular we mention the work by (von Rekowski & Brandenburg 2004) who in their simulations did not constrain the disk magnetic field but let it evolve by a dynamo process from an initial stellar magnetosphere. Indeed the disk magnetosphere evolves into an open field structure, however the radial profile of the disk field is not explicitly mentioned. The outflows from disk and star are pressure driven but a magneto-centrifugally driven outflow region co-exists originating in the inner part of the disk. However, no collimated jet flows have been observed in these simulations covering a area of 0.1×0.2 AU.

Some insight into the parameter space investigated in our simulations may be gained by comparing them to stationary models of accretion-ejection structure. As an example, in the following we discuss the solutions presented by Ferreira (1997). Ferreira et al. apply self-similar and stationary MHD for the disk-outflow system and derive the so-called ejection (or mass loading) index $\xi \equiv d \ln \dot{M}_{acc} / d \ln r$ as the leading parameter governing the structure of the outflow. They find this parameter being constrained by a lower limit of 0.004 due to the vertical disk equilibrium, and a maximum value $\xi < 0.15$ due to the condition of having a trans-Alfvénic jet⁵. Since by definition $\xi > 0$, it follows that $\mu_\rho < 3/2$. In fact, for $\mu_\rho = -3/2$ the Ferreira et al. approach gives the Shakura-Sunyaev disk density distribution and $\xi = 0$, i.e. a constant accretion rate $d\dot{M}_{acc}(r)$ and no outflow. Their upper limit $\xi = 0.15$ would imply a very narrow range for the radial density profile, $1.35 < \mu_\rho < 1.5$. However, in our simulations we obtain trans-Alfvénic outflows also for lower μ_ρ . Our interpretation is that this constraint might be an artifact of the self-similar approach undertaken by Ferreira et al. Without considering the disk structure self-consistently in a time-dependent simulation this question cannot be answered.

⁵Note that with $d\dot{M}_{acc}/dr \sim d\dot{M}_{jet}/dr$ we have $\mu_\rho = 3/2 - \xi$

The self-similar study further provides a constraint for the profile of the magnetic flux configuration $0 < \mu_\Psi < 2$ (note that β in Ferreira’s notation corresponds to μ_Ψ in our’s). This is in agreement with all parameter runs in our study. Another relation found by Ferreira et al. is that μ_Ψ can be related to ξ by $\mu_\Psi = 3/4 + \xi/2$, or $\mu = 1/2 + \mu_\rho/2$, respectively. (the number value $3/4$ indicates the Blandford-Payne solution). This quantifies the relation between the profile of the disk mass loss and that of the disk magnetic field. The above mentioned constraint $\mu_\rho < 3/2$ implies that $\mu < 5/4$, which tells us that our simulations in the upper part of Tab. 1 are inconsistent with the self-similar disk-jets discussed by Ferreira et al. However, considering the fact that (i) the steepness of the field profile is not so different from the other runs and that (ii) the analytical constraint is limited by the self-similarity assumption, we still think that these runs provide valuable scientific information.

Finally, we can only stress the point once more that both the the mass loading from disk into the outflow and the field structure will eventually defined by the disk physics and the constraints to it set by the existence of an outflow.

3.6. Jet flow magnetization

In ideal MHD the magnetic field is “frozen” into the matter which itself slides along (but not parallel to) the field lines. In an axisymmetric and stationary configuration the magnetic field lines are located on *magnetic flux surfaces* $\Psi(r, z)$ and the velocity vector can be expressed as $\vec{v} = k(\Psi)\vec{B}/\rho - r\Omega_F(\Psi)$, where $k(\Psi) = (d\dot{M}/d\Psi) = (\rho v_p/B_p)$ is the mass flow rate per magnetic flux surface and $\Omega_F(\Psi)$ the iso-rotation parameter⁶. One of the most important parameters for MHD wind theory is the *magnetization* parameter Michel (1969),

$$\sigma \equiv \frac{B_p^2 r^4 \Omega_F^2}{4\dot{M}c^3}, \quad (9)$$

where $\dot{M}(\Psi)$ is the mass flow rate within the magnetic flux surface Ψ . The magnetization is inverse to the mass load $\sigma \sim k^{-1}$. For outflows expanding in spherically *radial direction*, Michel (1969) derived an analytical relation between the asymptotic outflow velocity and the magnetization, $v_\infty \sim \sigma^{1/3}$ (Michel scaling). The outflow collimation results in a variation in the power index of the Michel scaling (Fendt & Camenzind 1996). Essentially, the magnetization summarizes the important parameters for launching a high velocity outflow – rapid rotation, strong magnetic field and/or comparatively low mass load. It will therefore

⁶For simplicity, the iso-rotation parameter Ω_F can be interpreted as the angular velocity of a magnetic field line. Both $k(\Psi)$ and $\Omega_F(\Psi)$ are conserved quantities along the magnetic flux surface.

be interesting to study also the influence of the magnetization *profile* across the disk wind on the collimation of this wind into a jet. Having prescribed a power law for the profiles of the disk wind initial poloidal velocity $v_{\text{inj}}(r) = v_{\text{inj}}v_{\text{Kep}}(r)$, the rotation $\Omega_{\text{F}}(r) = \Omega_{\text{Kep}} \sim r^{-3/2}$, the density and magnetic field profile, the disk wind magnetization profile $\sigma_0(r) \equiv \sigma(r, z=0)$ follows a power law as well,

$$\sigma_0(r) \sim \frac{B_{\text{p}}^2(r)}{\rho(r)} r^{-1/2} \sim r^{-(2\mu - \mu_{\rho} + 1/2)} \equiv r^{\mu_{\sigma}} \quad (10)$$

(hence, $\mu_{\sigma} = \mu_{\rho} - 2\mu - 1/2$). A choice of parameters as $\rho_{\text{inj}}(r) \sim r^{-3/2}$, $B_{\text{p}}(r, z=0) \sim r^{-1}$ (Ouyed & Pudritz 1997a; Fendt & Cemeljic 2002) will result in a radial disk wind magnetization profile $\sigma_0(r) \sim r^{-1}$. The self-similar Blandford & Payne model gives $\mu_{\sigma} = -3/2$. In a recent paper Pudritz et al. (2006a) have followed an approach similar to the present paper, varying the mass load $k(r)$ at the disk surface as $k(r) \sim r^{-1}, r^{-3/4}, r^{-1/2}, r^{-1/4}$. This would correspond to magnetization profiles as $\mu_{\sigma} = 1, 0.75, 0.5, 0.25$, respectively, a parameter space which is also covered in our paper.

4. Results and discussion

We have run a large number of MHD jet formation simulations covering a wide parameter range concerning both the disk wind poloidal magnetic field profile and the "injection" density profile along the disk surface (see Tab. 1). The results presented here are preliminary in the sense that not all simulation runs could be performed over time scales sufficiently long enough for the MHD outflow *as a whole* to reach the grid boundaries or to establish a stationary state. This is due to the large grid size in combination with steep gradients in the disk wind parameters which in general allow only for a weak outflow from large disk radii. Nevertheless, our results allow for a firm interpretation of the overall outflow structure and evolution in the MHD jet formation region. In most cases we have obtained a quasi-stationary state for the outflow within the inner region (over at least 50% of the grid). In some cases the nature of the outflow prevents that a stationary state can be reached.

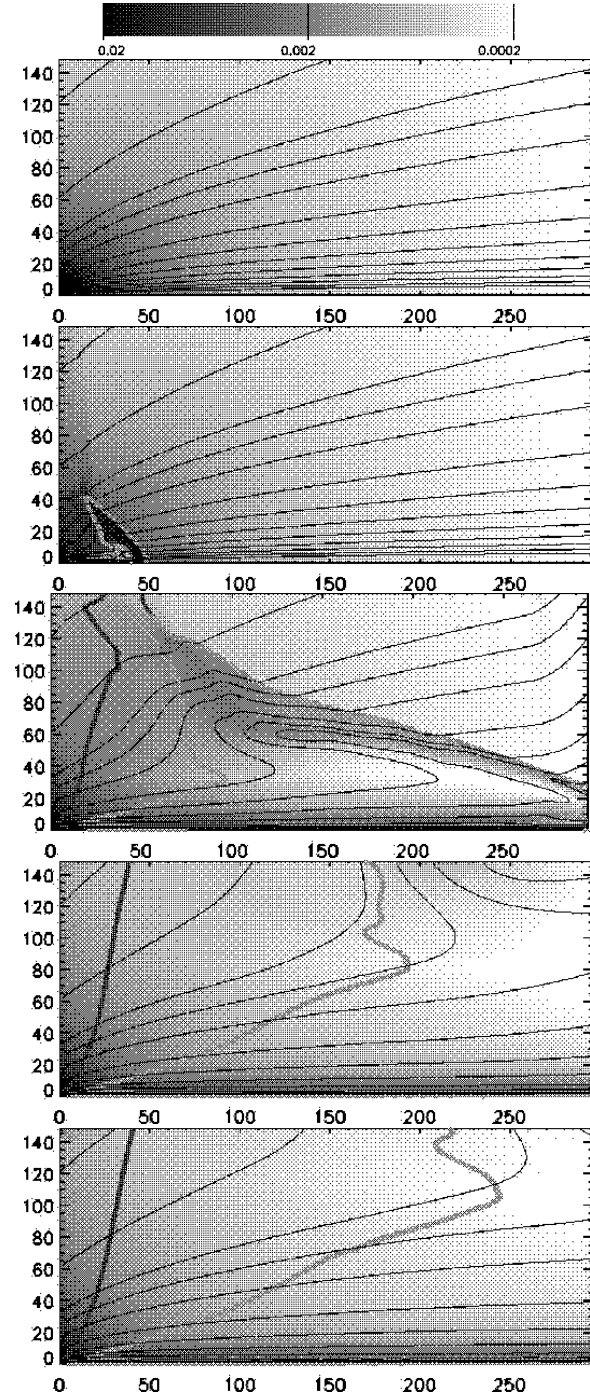


Fig. 1.— Simulation run i11. Mass density in *grey colors* (logarithmic scale between between the density values shown at the *color bar* on the very top) and poloidal magnetic field lines (*black lines*) at times $t = 0, 100, 500, 1500, 2090$ (from *top* to *bottom*). The r and z -axis point in vertical and horizontal direction, respectively. The dynamic range of the color coding is increased by setting densities above (below) the values given at the color bar to black (white). The thick dark grey and light grey contours indicate the run of the Alfvén surface and the fast magnetosonic surface, respectively.

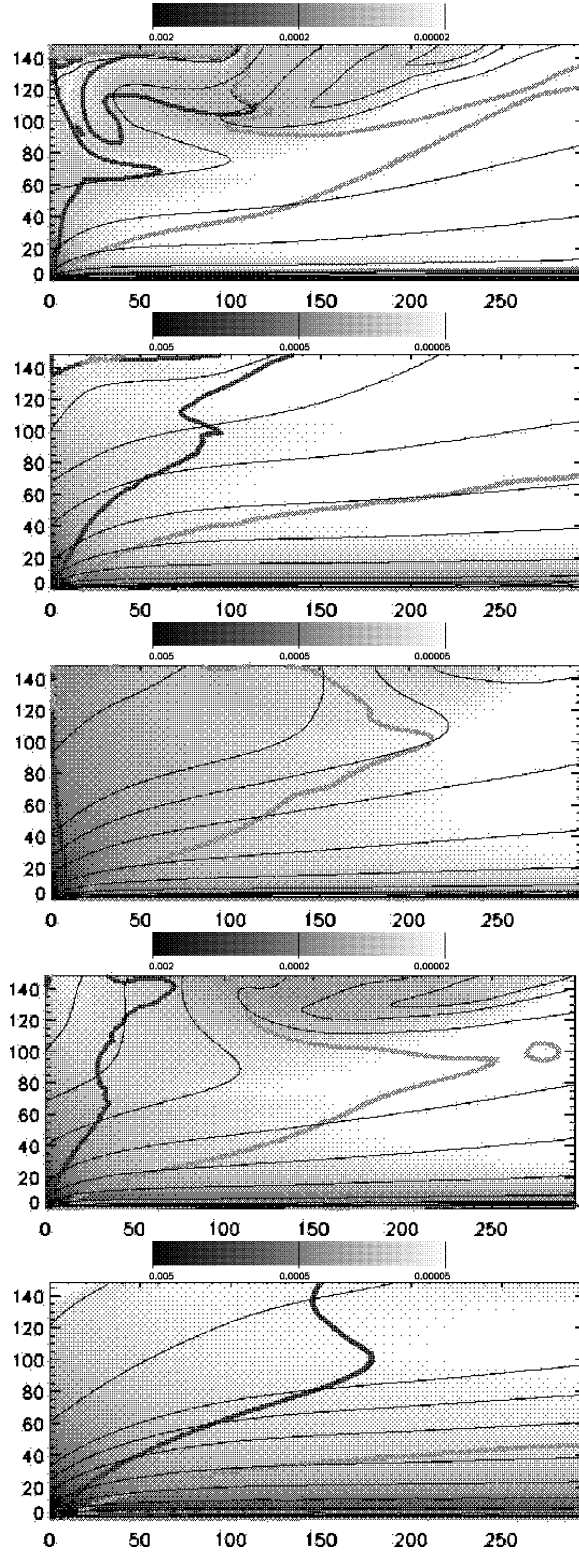


Fig. 2.— Simulation runs with different disk boundary conditions (see Tab. 1). Density and poloidal magnetic field lines for **p4** ($t = 2370$), **i15** ($t = 5000$), **p20** ($t = 1810$), **a2** ($t = 2000$), **i10** ($t = 3000$) from *top* to *bottom*. See Fig. 1 for further notation.

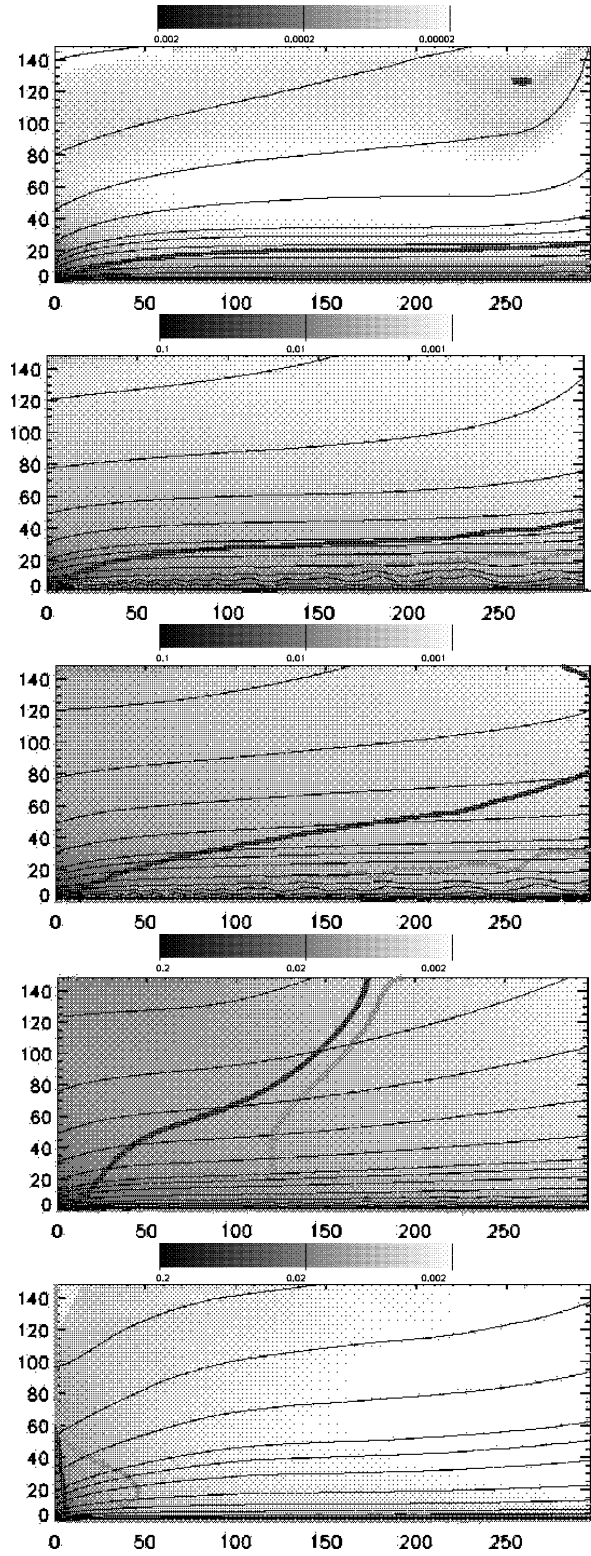


Fig. 3.— Simulation runs with different disk boundary conditions (see Tab. 1). Density and poloidal magnetic field lines for **p14** ($t = 1840$), **i2** ($t = 4000$), **i3** ($t = 4000$), **p16** ($t = 2790$), **c10** ($t = 1400$) from *top* to *bottom*. See Fig. 1 for further notation.

4.1. The general flow evolution

The main features of jet formation in the model scenario applied have been described in the previous literature (Ouyed & Pudritz 1997a, 1999; Fendt & Cemeljic 2002) and will not be repeated here in detail. In summary, the early evolution ($t < 100$) is characterized by the propagation of torsional Alfvén waves launched by the differential rotation between disk and corona (see Fig. 1). The Alfvén waves slightly distort the initial field structure into a new state of hydrostatic equilibrium which will remain stationary until reached by the MHD outflow launched from the disk. The region beyond the wave front remains undisturbed. Torsional Alfvén waves are still propagating across the grid, when the MHD wind begins to accelerate from the disk surface and becomes collimated beyond the Alfvén surface. The outflow rams into surrounding magnetohydrostatic corona developing a bow shock which propagates with velocities comparable to the material speed. The flow structure which is left when the bow shock has passed the computational grid is a pure disk wind/jet, generated and energetically maintained by the disk rotation, the continuous mass injection from the disk and the disk magnetic flux. We note that at these later evolutionary stages the outflow has completely swept out of the grid the initial condition and is governed solely by the boundary conditions.

As a general result, outflows launched from a flat disk magnetic field profile ($\mu < 0.5$) do not reach a steady state. Instead, a wavy pattern evolves close to the symmetry axis with almost constant mass flow rate in axial direction but variable mass flow rate in lateral direction. This case is similar to the extreme example of an initially *vertical* magnetic field examined by Ouyed & Pudritz (1997b).

Table 1: Summary table of our simulation runs. Shown are parameters for the disk poloidal magnetic field profile μ , the disk wind density profile μ_ρ , and the disk wind magnetization profile μ_σ . The inner disk radius poloidal field strength is $B_{p,i}$. The density at this radius is $\rho_{,i} = 1$, but is sometimes lowered by a factor of two (denoted by a \star in column 1). Mass flow rates in r - and z -direction along the three sub-grids $(r_{\max,i} \times z_{\max,i}) = (20.0 \times 60.0), (40.0 \times 80.0), (60.0 \times 150.0)$ are denoted as $\dot{M}_{z,i}, \dot{M}_{r,i}$, respectively. The average degree of collimation measured by the mass flow rates in z and r -direction, and normalized by the area threaded, is $\langle\zeta\rangle$. The maximum flow velocity obtained outside the axial spine is v_{\max} .

run	μ	μ_ρ	μ_σ	$B_{p,i}$	τ	$\dot{M}_{z,1}, \dot{M}_{r,1}$	$\dot{M}_{z,2}, \dot{M}_{r,2}$	$\dot{M}_{z,3}, \dot{M}_{r,3}$	$\hat{\zeta}_1, \hat{\zeta}_2, \hat{\zeta}_3$	v_{\max}	$\langle\zeta\rangle$
p21	1.5	2.0	-1.5	0.214	2010	0.25, 0.16	0.40, 0.07	0.42, 0.16	9.6, 22.8, 13.0	1.25	15
i9	1.5	2.0	-1.5	0.667	840	0.14, 0.28	0.37, 0.10	0.42, 0.16	3.0, 14.8, 13.0	3.08	15
c3	1.5	1.5	-2.0	0.214	1940	0.49, 0.36	0.78, 0.29	0.85, 0.30	8.4, 10.8, 14.0	1.07	15
p4	1.5	1.5	-2.0	0.321	2370	0.40, 0.46	0.72, 0.33	0.87, 0.41	5.2, 8.8, 11.0	1.74	10
i16	1.5	1.0	-2.5	0.321	2040	0.56, 1.51	1.21, 1.84	1.73, 2.12	2.2, 2.6, 4.0	2.50	5
i4, \star	1.5	0.5	-3.0	0.40	550	0.93, 2.10	1.88, 4.07	1.30, 7.07	2.7, 1.9, 0.92	1.47	2
i8	1.5	0.5	-3.0	2.67	290	0.11, 5.78			sup.-Alf. inflow		?
i14	1.25	1.5	-1.5	0.355	610	0.63, 0.49	1.01, 0.46	1.09, 1.40	7.8, 8.8, 4.0	1.53	10
i15, \star	1.25	1.5	-1.5	0.177	5000	0.25, 0.28	0.42, 0.24	0.52, 0.22	5.4, 7.2, 12.0	1.22	10
p20	1.25	1.0	-2.0	0.355	1810	1.07, 1.58	1.98, 2.00	2.31, 2.69	4.2, 4.0, 4.5	1.47	5
a2	1.25	0.5	-2.5	0.177	2350	0.56, 0.51	0.89, 0.69	1.03, 0.58	6.6, 5.1, 8.8	0.91	8
p2	1.0	1.5	-1.0	0.155	2550	0.79, 0.53	1.21, 0.40	1.43, 0.38	9.0, 12.0, 18.5	0.87	15
i10	1.0	1.5	-1.0	0.155	3330	0.75, 0.49	1.11, 0.49	1.32, 0.52	9.0, 9.2, 12.5	0.89	10
i11	1.0	1.0	-1.5	0.155	2090	1.60, 1.66	2.75, 2.13	3.18, 2.97	5.8, 5.2, 5.5	0.84	5
c9	1.0	0.5	-2.0	0.358	1730	3.14, 6.14	6.64, 11.5	8.30, 18.5	3.1, 2.3, 2.3		2
p13	0.8	1.5	-0.6	0.922	290	0.93, 0.53	1.87, 1.28	6.00, 1.90	10.5, 5.8, 15.8	2.33	15
p14	0.8	1.5	-0.6	0.307	1840	0.90, 0.46	1.34, 0.39	1.41, 0.43	12.3, 18.2, 16.5	1.18	20
a1	0.8	1.5	-0.6	0.247	2830	1.02, 0.35	1.39, 0.26	1.55, 0.34	17.5, 20.5, 22.8	1.08	20
i17	0.8	1.0	-1.1	0.247	2790	1.88, 1.49	3.44, 1.89	4.58, 1.59	7.6, 7.3, 14.5	1.05	$\simeq 15$
p15	0.8	0.6	-1.5	0.310	990	3.34, 4.60	6.95, 7.81	9.13, 11.2	4.4, 3.6, 4.1	1.05	4
c10	0.8	0.5	-1.6	0.247	1400	3.85, 6.08	8.05, 11.8	11.3, 18.8	3.8, 2.7, 3.0	0.93	3
i19	0.65	1.5	-0.3	0.279	1420	0.53, 0.17	0.73, 0.16	0.82, 0.27	18.4, 18.1, 15.5	1.01	20
i18	0.65	0.5	-1.3	0.279	1600	4.93, 5.58	10.8, 10.1	14.2, 16.6	5.3, 4.3, 4.3	1.01	4
a5	0.65	1.0	-0.8	0.279	1700	2.14, 1.51	3.79, 1.75	4.59, 2.22	8.5, 8.6, 10.1	1.05	10
p6	0.5	1.5	0.0	0.112	1800	1.18, 0.33	1.65, 0.23	1.82, 0.25	21.5, 28.7, 36.4		30
i1	0.5	1.5	0.0	0.112	3600	1.18, 0.04	1.35, -.048	0.92, 0.18	161, (112), 25.6	0.7	30
p7	0.5	1.5	0.0	0.225	1000	1.19, 0.30	1.63, 0.26	2.07, 0.51	23.8, 25.1, 20.3	0.86	20
c5	0.5	1.5	0.0	0.225	430	1.23, 0.39	2.44, 0.35	4.89, -0.22	18.9, 27.9, (111)	0.78	30
c8	0.5	0.8	-0.7	0.112	3800	3.66, 2.08	7.38, 2.40	10.1, 1.77	10.6, 12.3, 28.5	0.7	30
i2	0.5	0.8	-0.7	0.112	3800	3.69, 2.07	7.37, 2.38	10.3, 1.75	10.7, 12.4, 29.4	0.5	30
p8, \star	0.5	0.5	-1.0	0.112	3500	3.18, 2.35	7.19, 3.86	10.5, 5.10	8.1, 7.5, 10.3	0.65	10
i3, \star	0.5	0.5	-1.0	0.112	3900	3.13, 2.15	7.74, 3.10	11.3, 4.07	8.7, 10.0, 13.9	0.65	15
p18	0.5	0.5	-1.0	0.112	2210	5.60, 5.48	12.5, 9.57	17.6, 15.3	6.1, 5.2, 5.8	0.51	5
p19	0.5	0.5	-1.0	0.225	1640	5.88, 5.14	12.9, 9.09	17.2, 15.1	6.9, 5.7, 5.7	0.95	6
p16	0.5	0.3	-1.2	0.225	2790	9.60, 7.87	24.2, 15.2	36.8, 27.0	7.3, 6.4, 6.8	0.58	7
c11	0.35	1.5	0.3	0.366	1250	1.14, 0.25	2.23, 0.55	2.39, 1.20	27.4, 16.3, 10.0		$\simeq 10$
a4	0.35	1.0	-0.2	0.255	2000	3.02, 0.70	5.05, 1.04	7.75, -.39	25.9, 19.4, (99)		$\simeq 25$
a6	0.35	0.5	-0.7	0.255	1900	8.51, 2.44	18.8, 1.38	23.9, 3.47	20.9, 54.3, 34.3	0.8	> 30
a8	0.2	1.0	0.1	0.296	1950	2.62, 0.67	4.93, 0.61	7.64, -2.5	23.5, 32.3, (-19)		$\simeq 30$
a7	0.2	0.5	-0.4	0.296	2100	8.89, 2.05	15.7, 3.67	29.9, 5.72	26.0, 17.1, 26.1	0.68	$\simeq 25$

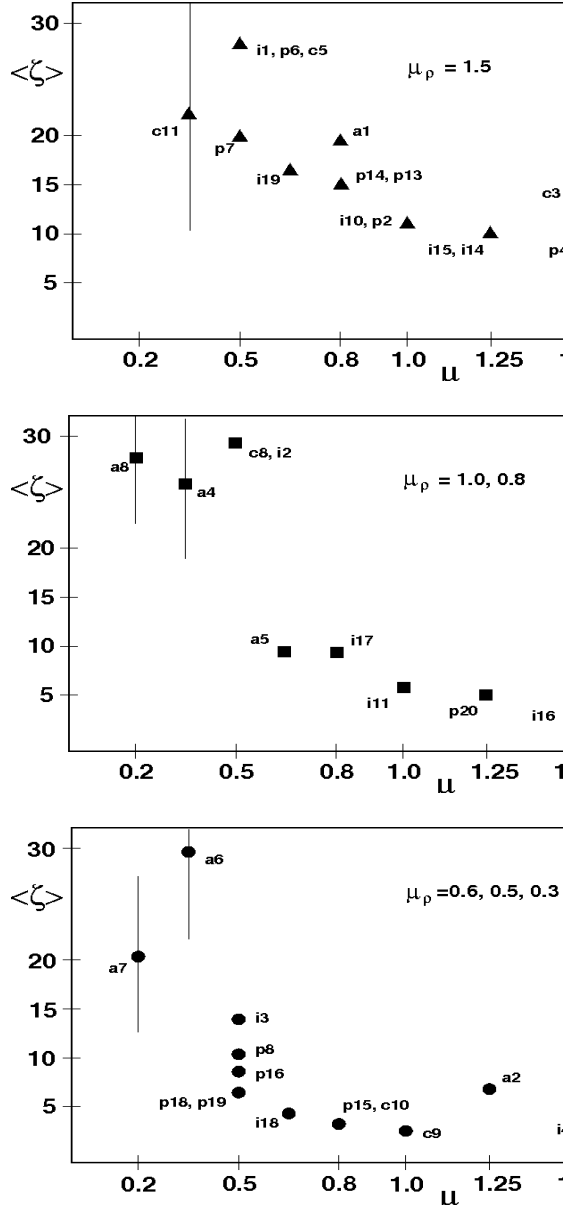


Fig. 4.— Degree of collimation measure (denoted by $\langle \zeta \rangle$) as defined in Sect. 4.2 and power law index of the disk poloidal magnetic field profile μ (see Tab. 1). The three sub-figures refer to simulations applying inflow density profiles, $\mu_\rho = -1.5$ (top), $\mu_\rho = -1.0$ (middle), $\mu_\rho = -0.5$ (bottom). Data points with bars indicate a variable collimation degree resulting in most cases from axial instabilities of highly collimated outflows.

4.2. How to measure the degree of collimation?

The main goal of this study is to investigate the relation between the accretion disk magnetic flux profile and the collimation of the outflow. In order to *quantify* such a relation we need to define a measure for the degree of outflow collimation. As a matter of fact, some ambiguity exists about such a definition and a few words of clarification are needed. What is usually observed as jet flow, is an elongated feature of radiation emitted in combination with a signature of high velocity. This is then associated with (i) an elongated mass distribution ("collimation") emitting the radiation and (ii) a strong axial velocity component ("acceleration"). Therefore, from the theoretical point of view, it is natural to apply the *directed mass flux as measure of jet collimation* (see below).

In this respect, we also note the different meaning of the "degree of collimation" and the "ability to collimate". The first term refers to the status of the established - collimated - outflow as directed mass flux which is probably equivalent to the observed jet. The second term refers to the question of how well an initially weakly collimated disk wind can be turned into a collimated stream by means of internal MHD forces. It is straight forward to expect that for the same disk magnetic field profile, a more concentrated disk wind density profile (i.e. large μ_ρ) will result in a more concentrated density profile of the asymptotic jet flow as well (presumably leading to a smaller jet radius observed). However, both a wide and a narrow jet, i.e. a jet with a flat or steep asymptotic density distribution, may have the same asymptotic opening angle (e.g. a cylindrical shape).

For ideal MHD jets in stationary state, collimation can be measured by the opening angle of the magnetic field lines. In the case of resistive jets, or if the outflow has not yet reached a steady state, this is not appropriate, as mass flux direction and magnetic field direction are not aligned.

In the present paper, we consider the *directed mass flux* as appropriate quantitative measure of outflow collimation. For simplicity, we measure the *degree of collimation* by the ratio ζ of mass flux in axial versus lateral direction,

$$\zeta \equiv \frac{\dot{M}_z}{\dot{M}_r} = \frac{2\pi \int_0^{r_{\max}} r \rho v_z dr}{2\pi r_{\max} \int_0^{z_{\max}} \rho v_r dz}. \quad (11)$$

This parameter depends on the size of the integrated volume. We determine the mass flow rates applying three differently sized volumes, $\dot{M}_{z,i}$, $\dot{M}_{r,i}$, considering different sub-grids of the whole computational domain of $150 \times 300 r_i$ corresponding to cylinders of radius and height $(r_{\max} \times z_{\max}) = (20.0 \times 60.0)$, (40.0×80.0) , (60.0×150.0) (see Tab. 1, Tab. 3, Tab. 2). We then consider the mass flux *ratio* ζ normalized to the size of the areas passed through by the mass flow in r- and z-direction, $\hat{\zeta}_1, \hat{\zeta}_2, \hat{\zeta}_3$. The ratio of grid size (r_{\max}/z_{\max}) as displayed

in our figures converts into a ratio of cylinder *surface areas* of $A_z/A_r \sim 0.5(r_{\max}/z_{\max})$. Thus, a mass flux ratio $\zeta_2 = 2$ as defined by Eq. (11) corresponds to a mass flux ratio normalized to the surface area threaded of $\hat{\zeta}_2 = 8$ which could be considered as “very good” collimation.

The difference in degree of collimation calculated for differently sized volumes, $\hat{\zeta}_1, \hat{\zeta}_2, \hat{\zeta}_3$, may also indicate different evolutionary states in different regions of the outflow. At a certain time, the outflow may already be well collimated close to its origin and also have reached a stationary state in this region. However, on larger spatial scales the same outflow may still interact violently with the ambient initial corona (see e.g. simulation runs c3, p4). Some simulations could be performed until an almost stationary flow on the whole numerical grid has developed (e.g. c8, p8). In other cases a quasi-stationary state of the outflow within the inner region (say 50% of the grid) has been reached. In most cases the initial corona has completely swept out of the grid. From the mass flow rates on the sub-grid we derive an *average degree of collimation* $\langle \zeta \rangle$ considered to be typical for that simulation, but depending on the evolutionary state of the flow.

We note another interesting consequence of the large grid applied compared to previous studies on smaller grid size (Ouyed & Pudritz 1997a; Pudritz et al. 2006a). In some of our simulations which reaches later evolutionary stages of the outflow the Alfvén surface leaves the grid in axial direction (see e.g. run i3). Thus, these outflows are sub-Alfvénic in their outer layers and the jet structure will consist of three nested layers (cylinders) of different magnetosonic properties – an outer sub-Alfvénic layer, a super-Alfvénic / sub-fast magnetosonic layer at intermediate radii, and a super-fast magnetosonic jet in the inner part (here we neglect the very inner axial spine where there is no mass inflow from the disk but potentially from a stellar wind). The extension of these layers depends on the parameters μ and μ_ρ and will be discussed in more detail below. For example, for simulation run i10, we estimate the asymptotic radius of the Alfvén surface to about $120r_i$, and the asymptotic radius of the fast magnetosonic surface to about $50r_i$. For comparison, in the original approach (Ouyed & Pudritz 1997a) passes the radial grid boundary at a height of about $z = 60$. A multi-layer structure of jets in respect to the magnetosonic surfaces has been proposed in stationary studies by Fendt & Camenzind (1996), however, then suggesting layering inverted to what we find now (ie. a super fast-magnetosonic flow in the outer part respectively). We expect that such a stratification in lateral direction should be essential for the jet stability. This particular issue has not yet been treated in the literature.

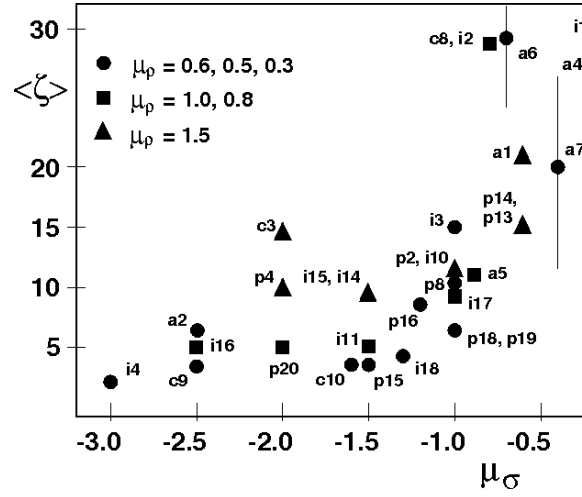


Fig. 5.— Degree of collimation (denoted $\langle \zeta \rangle$) as defined in Sect. 4.2 and power law index of the disk wind magnetization profile μ_σ (see Tab. 1). This figure combines all three sub-figures of Fig. 4 applying $\mu_\sigma = \mu_\rho - 2\mu - 1/2$. Data points with bars indicate a time variable collimation degree resulting in most cases from axial instabilities of highly collimated outflows.

4.3. Degree of collimation - MHD simulations

Simulation run i10 with $\mu = 1.0$, $\mu_\rho = 1.5$ serves as our “reference run” resembling just the same parameter set as applied in the exemplary solution by Ouyed & Pudritz (1997a), but now performed on a substantially larger physical grid. After $t = 3000$ (i.e. 3000 inner disk orbits) a stationary outflow is obtained over a large fraction of the grid. The run of the Alfvén surface at large radii indicates that the outermost layers of the outflow have not yet reached a stationary state (see Fig.2). We obtain degrees of collimation of $\hat{\zeta}_{1,2,3} = 9.0, 9.2, 12.5$ resulting in an “average” degree of collimation of $\langle \zeta \rangle = 10$ (see Tab. 1). As the outflow has not yet settled in a stationary state over the whole grid, these values will vary *slightly* for later times. Note that even 3000 orbits of the inner disk correspond to about only two orbits at the outer disk radius at $150 r_i$. The sequence $\hat{\zeta}_{1,2,3}$ also indicates an *increasing degree of collimation* along the outflow.

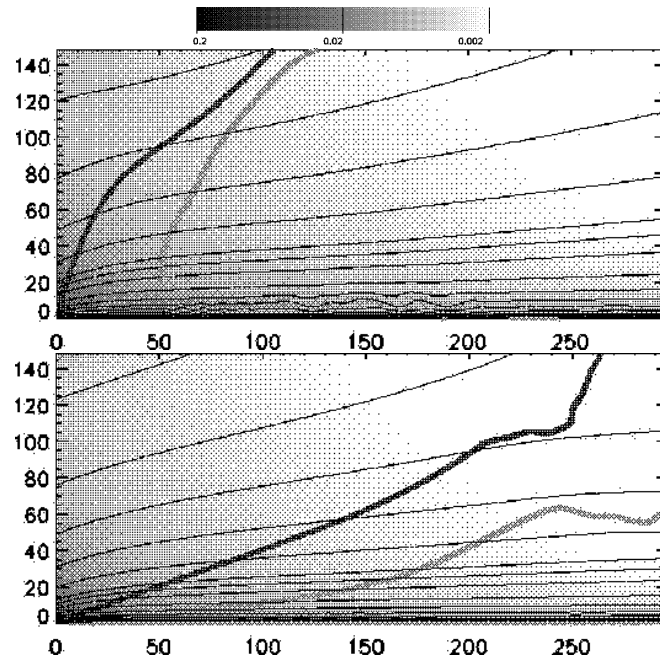


Fig. 6.— Simulation runs with different disk boundary conditions (see Tab. 1). Impact of a total disk magnetic flux variation (factor 4). Density and poloidal magnetic field lines for **p18** ($t = 2210$), **p19** ($t = 1640$) from *top* to *bottom*. See Fig. 1 for further notation.

4.3.1. Disk magnetic field profile and collimation

We now compare simulation runs with different disk magnetic flux profile μ, μ_Ψ , but similar inflow density profile μ_ρ . We have run about 40 different simulations which in total required about one year of CPU time on various work stations.

Table 1 shows the main input parameters for the each simulation run, in particular the power law index of the magnetic field and density distribution. Table 1 further shows the main parameters of the resulting outflow, namely the mass flow rates in lateral and axial direction defining the collimation degree. What is also indicated is the physical time step τ at which the mass flow rates are calculated. This is in most cases, but not always, the final time step of the simulation. When comparing different simulation runs, one has to keep in mind that they evolve with different dynamical speed. Thus, if possible, only outflows at late (or equivalent) evolutionary stages will be compared, which may have been reached after different physical time (as e.g. stronger magnetized outflows evolve faster, see below).

In general, we find an increasing degree of collimation with decreasing slope of the disk magnetic field profile⁷ (see Fig. 4). This holds for all of the disk wind density profiles investigated so far. A steep density profile generally leads to a higher degree of jet collimation which is, however, not surprising as the mass flux is more concentrated along the axis just by definition of the boundary condition.

For the simulations with relatively flat density profile ($\mu_\rho = 0.3, \dots, 1.0$), a strong increase in collimation degree can be observed just below $\mu = 0.6$. However, simulations with a flat disk magnetic field profile (below $\mu = 0.5$) do not reach a stationary state within the time scale of our simulations. In general, the degree of collimation for these outflows is high. The axial mass flow rate stays more or less constant whereas the radial mass flux varies in time, resulting in a "wavy" pattern evolving along the outflow axis. This has been discussed by Ouyed & Pudritz (1997b) for the case of an initially vertical coronal magnetic field and in the context of knot generation in protostellar jets.

Now we compare our results obtained for the different density profiles *quantitatively*. We find that a physically meaningful classification can be achieved by shifting and spreading the three figures (Fig. 4) not in vertical but in horizontal direction. Essentially, this corresponds to a comparison *collimation degree versus magnetization* by applying $\mu_\sigma = \mu_\rho - 2\mu - 1/2$. Indeed, the resulting diagram (Fig. 5) shows a convincing correlation between the magne-

⁷The mass flow rates in simulations with flat magnetic field profile $\mu < 0.4$ are difficult to determine as these outflows do not reach a stationary state and show a time-dependent variation in the lateral mass flux close to the axis

tization profile power law index μ_σ and the degree of collimation obtained $\langle \zeta \rangle$. As we naturally expect that the inflow parameters will change during the life time of an accretion disk, our results might explain why not all accretion disks do launch a jet and why disks do not launch jets for all their life time.

The above mentioned steep rise in collimation degree for $\mu < 0.6$ is now indicated for a magnetization profile $\mu_\sigma > -1.0$. Obviously, the slope of this rise depends in particular on the reliability of simulation runs a6, c8 and i2. We note that simulation i2 and c8 follow a relatively flat density profile, and did evolve up to several 1000 disk orbital periods into an almost stationary state on a global scale. Simulation a6 remains sub-Alfvénic over most of the grid size and has developed an instable flow pattern along the jet axis.

The width of the $(\mu_\sigma - \langle \zeta \rangle)$ -correlation shown in Fig. 5 is due to detailed differences in the parameter setup. The data points shown for a certain simulation which is deviating from the general trend of the correlation indeed have a particular origin. For example, simulation run c3 is strongly magnetized with the Alfvén surface very close to the r -axis. The same holds for simulation run i4. Therefore, both simulations do not consider a typical Blandford-Payne magneto-centrifugally launched jet, but have the Alfvén points close to the foot points of the field lines (hence a short lever arm). However, in summary we conclude that the numerical data give a clear correlation between the power law index of the disk wind magnetization profile and the degree of collimation.

Table 2: Summary of simulation runs obeying an artificial decay of the toroidal field component. The parameter f_{B3} gives the factor by which the toroidal magnetic field is artificially decreased each time step (see Tab. 1 for other notations).

run	μ	μ_ρ	μ_σ	$B_{p,i}$	τ	f_{B3}	$\dot{M}_{z,1}, \dot{M}_{r,1}$	$\dot{M}_{z,2}, \dot{M}_{r,2}$	$\dot{M}_{z,3}, \dot{M}_{r,3}$	$\hat{\zeta}_1, \hat{\zeta}_2, \hat{\zeta}_3$	v_{mx}	$\langle \zeta \rangle$
p10	1.5	0.8	-2.7	0.40	1800	0.1	-.04, 1.58	0.07, 2.45	0.11, 3.19	(0.2), 0.1, 0.2	0.18	0
p11	1.5	0.8	-2.7	1.20	3100	0.1	-.051, 1.59	0.057, 2.47	0.064, 3.40	(0.2), 0.1, 0.1	0.17	0
p17	1.0	1.5	-1.0	0.232	1890	0.9	0.30, 1.08	0.82, 0.97	0.96, 1.39	1.7, 3.4, 3.4	0.17	3
i12	1.0	1.0	-1.5	0.387	1520	0.9	0.60, 2.65	1.73, 3.20	2.59, 5.66	1.4, 2.2, 2.3	0.29	2
i13	1.0	1.0	-1.5	0.246	1020	0.9	.092, 3.19	1.33, 3.73	3.48, 7.38	0.17, 1.4, 2.4	0.32	2
p12	0.8	1.5	-0.6	0.922	870	0.9	0.87, 0.69	1.55, 1.19	1.26, 1.75	7.6, 5.2, 3.6	0.27	4

4.3.2. Field strength and collimation

While the slope of the disk magnetic flux / magnetization profile clearly governs the asymptotic collimation of the outflow, the amount of total disk magnetic flux is seemingly less important. We have investigated different absolute magnetic fluxes for the same flux profile and did not detect any relation with the degree of collimation. Simulations with high magnetic field strength are CPU time consuming due to the Alfvén speed time stepping. On the other hand, the jet evolves faster and also propagates across the numerical grid within a shorter period of time (physical units). We thus reach similar evolutionary stages at earlier physical time (but after more numerical time steps).

For reference we compare simulation runs i14 and i15 with field strength $B_{p,i}(i15) = 0.5B_{p,i}(i14)$ and initial flow density $\rho_{inj}(i15) = 0.5\rho_{inj}(i14)$; runs p13, p14 and a1 with $B_{p,i}(p13) = 3.0B_{p,i}(p14) = 3.73B_{p,i}(a1)$ and $\rho_{inj}(i15) = 0.5\rho_{inj}(i14)$; and runs p18, and p19 with $B_{p,i}(p19) = 2.0B_{p,i}(p18)$ (see Fig. 6). Table 1 shows that the collimation degree is indeed similar for each example, as it is the evolving jet structure (see examples p18 and p19, Fig. 6). On the other hand, the total magnetic flux governs the asymptotic velocity gained by the jet (see below).

4.4. Jet collimation for highly diffusive toroidal field

As mentioned above (Sect.2.3), studies in the literature have proposed a ”poloidal collimation” of the jet, i.e. jet collimation due to the pressure of an ambient poloidal magnetic field (Spruit et al. 1997; Matt et al. 2003). In order to investigate the feasibility of such a process, we have performed a set of simulations applying an artificially strong decay of the toroidal field component, invented to mimic the toroidal field decay due to the kink-instability (Spruit et al. 1997).

Our simulations (see Tab. 2) follow a parameter setup equivalent to those in Tab. 1 with the single exception that the toroidal field is artificially decreased by either a factor $f_{B3} = 0.9$ or 0.1 at each numerical time step⁸. Thus, this part of our paper considers a ”toy model” mimicking an artificially enhanced magnetic diffusivity, only affecting the toroidal field component⁹. A fully self consistent approach would involve a tensorial description of

⁸This is done in the ZEUS subroutine ”ct” treating the constrained transport and updating the magnetic field components

⁹We note that the artificial toroidal field decay sometimes causes problems for the usual outflow boundary condition in axial direction. However, so far the internal structure of the outflow has not been not affected

magnetic diffusivity with strong diffusivity for those components affecting the toroidal field component. This is beyond the scope of the present paper.

During the long-term evolution of these outflows the resulting toroidal magnetic field is decreased by 5 orders of magnitude compared to the simulations presented before (independent of f_{B3}). The simulation runs we have to compare are p17 with p2 and i10, runs i12 and i13 with i11, run p12 with p14 and p13, and runs p10 and p11 with i16. All outflows with decaying toroidal magnetic field are substantially less collimated (Tab. 2). This is not surprising as the collimating tension force by the toroidal field has just been switched off. The exception is simulation run p12 which, due to its steep disk wind density profile, shows relatively good collimation comparable to the previous simulations runs without toroidal field decay.

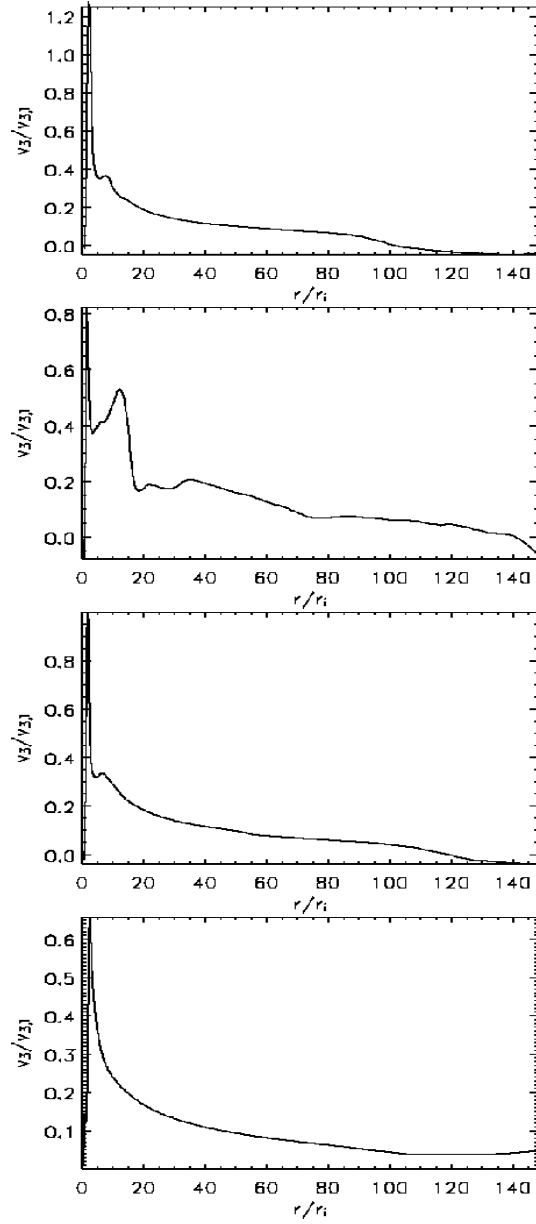


Fig. 7.— Toroidal velocity profile across the jet at $z = 160$ for selected parameter runs at the final stages of simulation. **i3** ($t = 4000$), **i1** ($t = 3000$), **p8** ($t = 3200$), **i11** ($t = 2000$) from *top* to *bottom*.

4.5. Jet velocity & Michel scaling

In general we obtain a narrow range for the maximum velocity of the super-Alfvénic flow at large distance from the origin. The maximal jet velocity is typically in the range of the Keplerian speed at the inner disk radius, in agreement with the literature (Ouyed & Pudritz 1997a; Casse & Keppens 2002; Kudoh et al. 2002). However, in our simulations we noticed a slight trend in the jet velocity in relation to the magnetization σ . In order to further investigate the Michel scaling for collimated jets, we have performed simulation runs with identical initial field and mass flow *profile*, but different absolute number values for mass flow *rate* and magnetic field *strength* - either varying the initial magnetic field strength or the inflow density by a certain factor.

These simulations are summarized in Tab. 3. In particular, we may compare simulations p21 to i9, c3 to p4, i14 to i15, p13 to p14 and a1, i1 to p7 and c5, and p18 to p19 (see Fig.6). Table 3 shows the ratio of the maximum poloidal velocity for either of the simulations (labeled as 'A' and 'B') as expected from the original Michel scaling

$$\mathcal{R}_v \equiv \frac{v_{\infty,A}}{v_{\infty,B}} = \left(\frac{\sigma_A}{\sigma_B}\right)^{1/3} = \left(\frac{B_{p,A}}{B_{p,B}}\right)^{2/3} \left(\frac{\sigma_{i,A}}{\sigma_{i,B}}\right)^{1/3}, \quad (12)$$

and each of the numerical values involved (iso-rotation Ω_F and injection velocity are the same for all examples). The jet velocity has been measured along a slice across the jet at $z = 160$. The poloidal velocity profile has a maximum close to the axis. For each sample, the velocity measure of the asymptotic flow has been taken at similar spatial location and comparable evolutionary time step. This is an important point as we compare simulations which different evolutionary time scales where in some cases the large scale flow has not yet settled in a steady state.

The situation for the toroidal velocity is less pronounced. The typical rotation velocity at ($z = 160, r = 80$) is 1/10 of the Keplerian speed at the inner disk for most of the cases investigated. Examples for toroidal velocity profiles across the jet are shown in Fig. 7.

Our large-scale numerical grid allows for direct comparison of the numerically derived velocity structure with recent observations indicating rotation in the jet from the young stellar object DG Tau (Bacciotti et al. 2002). The numerical grid covers about 7×14 AU which is about the size of the innermost slit position shown in Fig.7 of Bacciotti et al. (2002). These authors measure radial velocities up to 400 km/s and find two major outflow components - a low velocity and a high velocity component. It is the low velocity component of de-projected¹⁰ jet velocity of about 90 km/s which shows radial velocity shifts of up to

¹⁰Assuming an inclination of 38° , see (Bacciotti et al. 2002) and references therein

12 km/s. The radial velocity differences across the jet have been widely interpreted as indication of rotation although this is not yet completely confirmed. The observed velocity data corresponding to our numerical grid (equivalent to "Slit S3/S5" and "Region I" in Bacciotti et al. (2002)) are 64 km/s in poloidal velocity (in [SII]) and 8 km/s as total radial velocity shift. The Keplerian speed at the inner disk radius for DG Tau is

$$v_{K,i} = 113 \text{ km/s} \left(\frac{M}{0.67 M_{\odot}} \right)^{1/2} \left(\frac{R_i}{10 R_{\odot}} \right)^{-1/2}, \quad (13)$$

assuming a central mass of $0.67 M_{\odot}$ (see Bacciotti et al. (2002) and references therein). According to such a normalization, our simulations which fit best to the low velocity jet of DG Tau are those with a flat magnetic field profile $\mu \simeq 0.5$ and with moderate field strength, namely i1, ..., p8 (see Tab. 1) These runs also show a high degree of collimation which is observed as well. The numerically derived rotational velocity for these examples is about $0.1 v_{K,i} \sim 10$ km/s which is surprisingly close to the observed value (see Fig. 7). The launching radius can then be derived just by following back the streamlines along the collimating jet flow. In the runs i1, ..., p8 the launching region is distributed over a relatively large disk area of $r \lesssim 80$ corresponding to about 3 AU. Note that in these simulations only the inner part of the jet is super-Alfvénic. Note also that the toroidal velocity in the numerical models *decreases* with radius in apparent contradiction with the observations of DG Tau (which, however, do not resolve the region close to the axis). We like to emphasize that in a self-consistent picture also the high velocity component has to be explained by the same simulation. As another note of caution we mention that all MHD simulations of jet formation done so far have shown a terminal jet speed of the order of the Keplerian speed at the launching region (Ouyed & Pudritz 1997a, 1999; Fendt & Cemeljic 2002; Vitorino et al. 2003). It is therefore difficult to interpret the very high velocity 450 km/s features observed for DG Tau in such a framework unless we assume very strong magnetic flux respectively a very low mass loading.

We finally discuss briefly the outflow velocities obtained in simulations with strongly diffusive toroidal field. As seen from Tab. 2, the typical velocities in such outflows are about a factor 5 lower compared to the standard approach. In particular, this follows from comparing simulations p2 to p17, i11 to i12 and i13, and p13 to p12. This is not surprising as we have artificially reduced the accelerating Lorentz force component (along the field), $\vec{F}_{L,\parallel} \sim \vec{j}_{\perp} \times \vec{B}_{\phi}$, where \vec{j}_{\perp} is the poloidal electric current density component $\vec{j}_{\perp} \sim \nabla \times \vec{B}_{\phi}$ perpendicular to the magnetic field.

Table 3: Subset of Tab. 1, summarizing simulation runs with similar field and density profiles but different relative magnetic flux. For the notation of the jet velocity ratio $\mathcal{R}_v \equiv v_{\infty,A}/v_{\infty,B}$ and the magnetization ratio $\mathcal{R}_\sigma \equiv \sigma_A/\sigma_B$ we refer to the text and Eq. 12.

run	μ	$B_{p,i}$	ρ_i	v_{mx}	$\langle \zeta \rangle$	$\mathcal{R}_\sigma^{1/3}$	\mathcal{R}_v
c3	1.5	0.214	1.0	1.07	15	1.31	1.63
p4	1.5	0.321	1.0	1.74	10		
i14	1.25	0.355	1.0	1.53	10	1.26	1.25
i15	1.25	0.177	0.5	1.22	10		
p13	0.8	0.922	1.0	2.33	15	2.08	1.98
p14	0.8	0.307	1.0	1.18	15	1.17	1.09
a1	0.8	0.247	1.0	1.08	15		
i1	0.5	0.112	1.0	0.7	30	1.59	1.23
p7	0.5	0.225	1.0	0.86	20		
c5	0.5	0.225	1.0	0.78	30		
p18	0.5	0.112	1.0	0.5	5	2.13	2.46
p19	0.5	0.225	1.0	0.95	6		
p16	0.5	0.225	1.0	1.1	7		

4.6. The run of the Alfvén surface

Another parameter which measures the relative strength of the magnetic field is the Alfvén Mach number M_A ,

$$M_A^2 \equiv \frac{4\pi\rho v_p^2}{B_p^2} \quad (14)$$

At the inflow boundary (= disk surface) the Alfvén Mach number varies as

$$M_{A,0}^2(r) \sim r^{2\mu-\mu_\rho-1} \sim r^{-\mu_\sigma-3/2} \equiv r^{-\mu_A}, \quad (15)$$

with $\mu_A = \mu_\sigma + 3/2$. A classical Blandford-Payne type MHD jet is launched as slow sub-Alfvénic disk wind, i.e. $M_{A,0}(r) < 1$ for all radii along the disk surface. In turn, this condition constrains the disk wind poloidal magnetic field and density profile, respectively, $\mu_\rho > 2\mu + 1$. For smaller μ , a situation may occur that at a certain radius the disk wind will be launched as *super-Alfvénic* flow. The location of this radius depends on the actual values of $B_{P,i}$ and ρ_{inj} . Therefore, in general sub-Alfvénic disk winds require a positive exponent for the $M_A(r)$ profile. In the self-similar Blandford & Payne approach we have $\mu_\sigma = -3/2$, while in the Ouyed & Pudritz (1997a) simulations $\mu_\sigma = -1$. A dipolar (stellar) magnetic field distribution with $\mu_\rho \sim 3/2$ implies $\mu_\sigma = -1$ and, thus, $M_{A,0}(r) \sim r^{-1/4}$, that means a critically negative exponent. The disk wind launched will be super-Alfvénic (Fendt & Elstner 2000).

Note that the relation between the magnetization σ and the collimation measure $\langle \zeta \rangle$ shown in Fig. 5 holds similarly for the Alfvén Mach number as $\mu_A = \mu_\sigma + 3/2$.

Figure 8 summarizes our results concerning the shape of the Alfvén surfaces in respect of outflow collimation degree. The showcase plot indicates the run of the Alfvén surface of different simulations, overlaid by the numerically observed degree of collimation for these outflows (indicated by ellipsoidal areas). Only examples with a sub-Alfvénic disk wind profile were chosen for this figure. In general, a "flat" Alfvén surface (i.e. curving towards the r -direction) indicates a less collimated jet. Some of these outflows are not fully evolved dynamically on a global scale, but as we measure the collimation degree only within $r = 150$, the main results derived are nevertheless reliable. For highly collimated outflows the Alfvén surface curves parallel to the jet axis already at rather low altitudes above the disk.

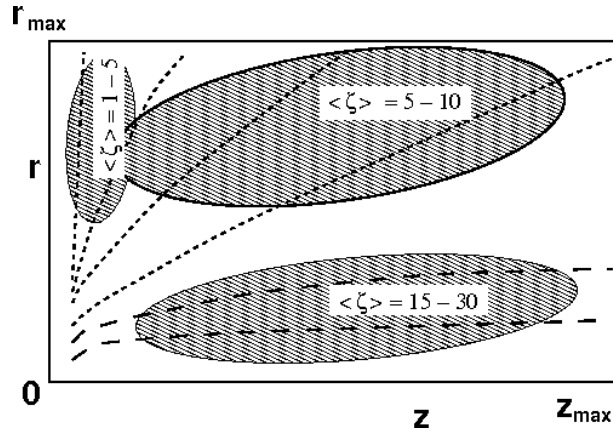


Fig. 8.— Showcase run of Alfvén surfaces for different simulation runs (see Figs. 2, 3, 6, 9). Selected are simulations: p20, i16; a2, i11, p4; p19, p16, p15, i15; i3, i10; i2, i9; p7, i1, p14 (clockwise from r -axis). The shape of the Alfvén surfaces is governed by the parameters μ and μ_ρ . Dashed/dotted lines highlight Alfvén surfaces leaving the grid through the z -boundary / r -boundary. As indicated by the ellipsoids, the latter ones are typical for highly collimated outflows, the first ones for less collimated outflows. Only examples with a sub-Alfvénic disk wind profile were chosen for this figure.

We have also extreme examples (i5, i8) for which the Alfvén surface curves towards the equatorial plane (see Fig. 11 for i8) such that the outer part of the disk wind is launched super-Alfvénic. Those winds cannot not *magneto-centrifugally* accelerated but are *magnetically* driven by the Lorentz force in vertical direction, $\vec{F}_{L,z} \sim \vec{j}_r \times \vec{B}_\phi + \vec{j}_\phi \times \vec{B}_r$. Note that simulations i15 and p20 seemingly look similar to the case of a super-Alfvénic disk wind, but actually start as sub-Alfvénic disk wind everywhere as resolved by our scaled grid.

The kink in the Alfvén surface in simulation i10 (Fig. 2, *bottom*) demonstrates that the outer part of the outflow has not yet reached a stationary state. The foot point radius of that flux surface intersecting the kink is at about $50 r_i$. Similarly, this holds for most of the other simulation runs.

5. Summary

We have performed numerical MHD simulations of jet formation from accretion disks. The disk is taken as a time-independent boundary condition determining the disk magnetic flux profile and the density profile of the mass flux from the disk surface. This implies that we implicitly assume that disk internal physical processes such as diffusion, advection, or turbulence have worked together in generating and maintaining a large scale disk magnetic field structure which leading to a disk surface field profile and the mass flux profile as prescribed in our simulations. The underlying assumption is that a variation of internal disk parameters can lead to a variation in the resulting magnetic and mass flux profile.

We applied the ZEUS-3D MHD code in the axisymmetric option and modified for physical magnetic diffusivity. Our physical grid size is (150×300) inner disk radii corresponding to about (6.7×13.3) AU for $r_i \simeq 10 R_\odot$ in the case of a protostellar jet which is several times larger than in previous studies in the literature and comparable to the observational resolution. We applied a simple parameterization for physical magnetic diffusivity in which turbulent Alfvénic pressure is responsible for both turbulent magnetic diffusivity and pressure. However, the magnitude of magnetic diffusivity is well below the critical value derived earlier beyond which the degree of jet collimation becomes affected (Fendt & Cemeljic 2002).

The major goal of this paper was to investigate if and how the jet collimation depends on the accretion disk magnetic flux profile. As a quantitative measure of the collimation degree we apply the directed mass flux (axial direction versus lateral direction). We have run a substantial number of simulations covering a large area in the parameter space concerning the mass flux and magnetic flux profile across the jet. In particular, we varied

- the disk poloidal magnetic field *profile* parameterized by a power law $B_p(r) r^{-\mu}$,

- the disk wind density *profile* (i.e. the density "injected" from the disk surface into the jet flow) parameterized by a power law $\rho_p(r) r^{-\mu_p}$,
- the disk magnetic field strength and/or the total mass flux.

This corresponds to a variation of the *mass flux profile* across the jet, the *magnetization profile* across the jet, and the magnetosonic *Mach number* across the jet.

Our simulations give clear evidence that a flatter magnetic field profile in the disk wind generally leads to a higher degree of jet collimation. This holds for all density profiles applied, however, the collimation degree increases with increasing slope of the density profile. For very flat magnetic field profile ($\mu \lesssim 0.4$) the jet flows do not settle into a stationary state. Instead, instabilities evolve along the outflow axis.

Furthermore, we find a unique correlation between the slope of the disk wind magnetization profile and the degree of jet collimation, potentially explaining why not all accretion disks do launch a jet and why a disk does not launch jets for all its life time.

A variation of the total magnetic field strength does not seem to affect the degree of collimation (at least not for a variation by factors up to 8 we investigated). The same holds for the total mass flux in the jet flow. However, the relative field strength affects the time scale for the dynamical evolution of the outflow - jets with stronger magnetic flux evolve faster.

Comparing simulations with different magnetization but the same magnetic flux profile we were able to prove the Michel scaling (Michel 1969) for the asymptotic outflow velocity $v_\infty \sim \sigma^{1/3}$ with relatively good agreement. The small deviations may be explained by the fact that we investigate collimated and not spherical outflows and also outflows which are to some part still dynamically evolving on the global scale.

In order to prove the feasibility of "poloidal collimation" which has been discussed in the literature, we invented a toy model introducing artificial decay of the toroidal magnetic field component (in addition to our parameterization of physical magnetic diffusivity). In general, such outflows show less collimation and also reach only lower asymptotic speed. However, as a matter of fact, outflow collimation is definitely present even in the absence of toroidal fields.

Comparing our numerical results to observations of DG Tau we find indication for a flat magnetic field profile in this source, as in this case the observed and the numerical jet velocity (low velocity component) and jet rotation do match.

In summary, our paper clearly states a correlation between the disk wind *magnetization*

profile and the *outflow collimation*. Good collimation requires a flat magnetization profile across the jet, i.e. sufficient magnetization also for larger disk radii. The final solution to the question of the jet mass loading and the disk-jet magnetic field structure is expected to come from simulations taking into account self-consistently both the internal disk dynamics and the outflow.

I thank the LCA team and M. Norman for sharing the ZEUS code. H. Zinnecker and J. Wambsganss are thanked for financial support during the time in Potsdam when most of the computations for the present paper were performed.

A. Figures intended for electronic publication only

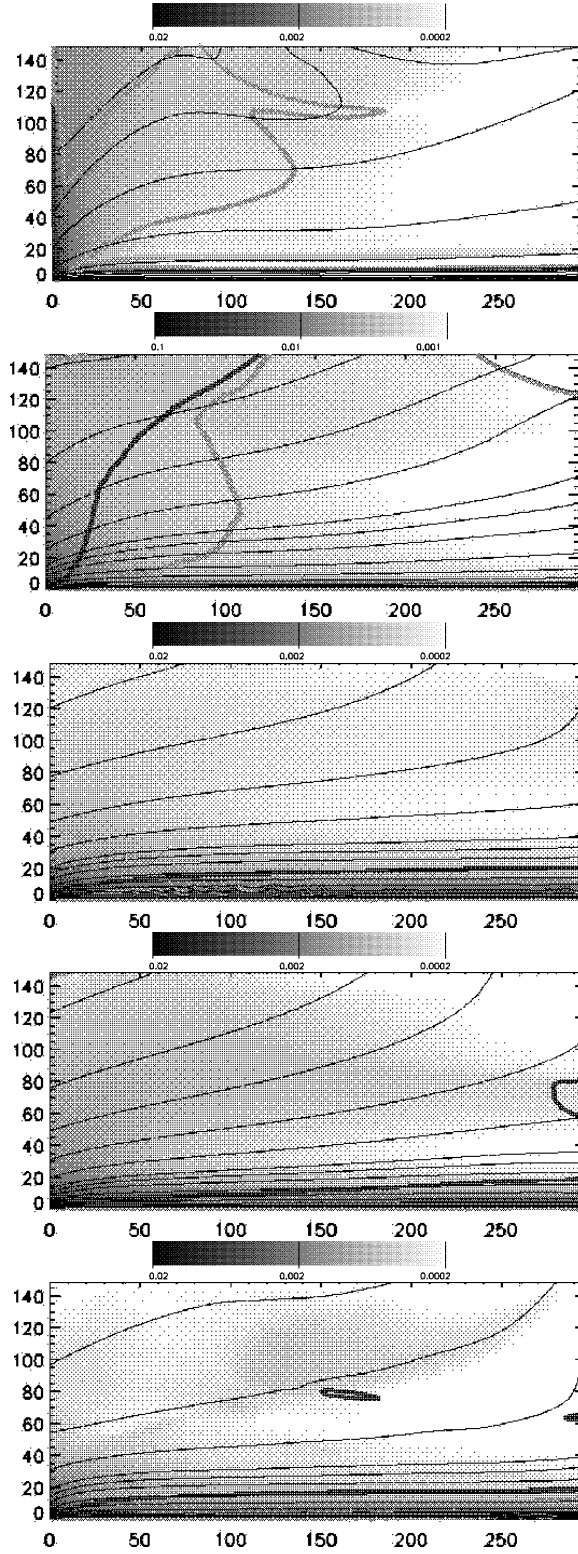


Fig. 9.— Simulation runs with different disk boundary conditions (see Tab. 1). Density and poloidal magnetic field lines for **i16** ($t = 2040$), **p15** ($t = 990$), **i1** ($t = 2000$), **p7** ($t = 1000$), **a1** ($t = 2830$), from *top* to *bottom*. See Fig. 1 for further notation.

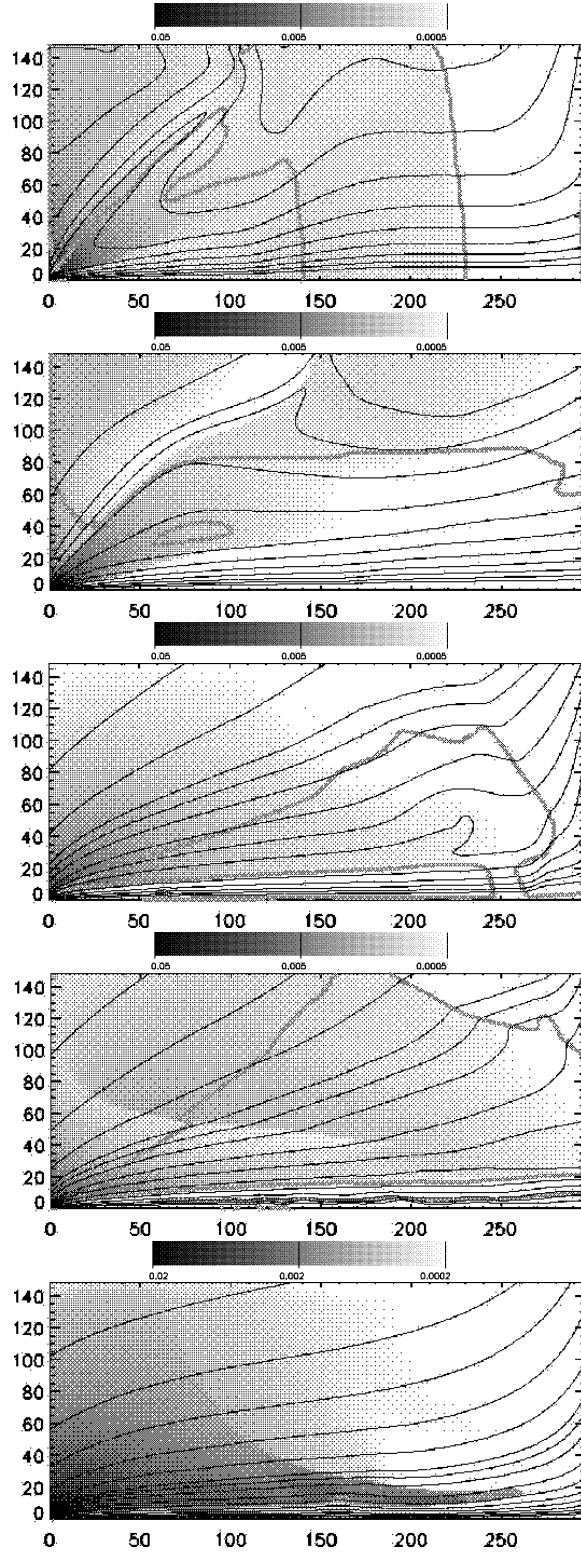


Fig. 10.— Simulation runs with different disk boundary conditions (see Tab. 2). Enhanced magnetic diffusivity for the toroidal magnetic field component B_ϕ . Density and poloidal magnetic field lines for **p10** ($t = 1800$), **p11** ($t = 3100$), **p17** ($t = 1890$), **i12** ($t = 1520$), **p12** ($t = 870$) from *top* to *bottom*. See Fig. 1 for further notation.

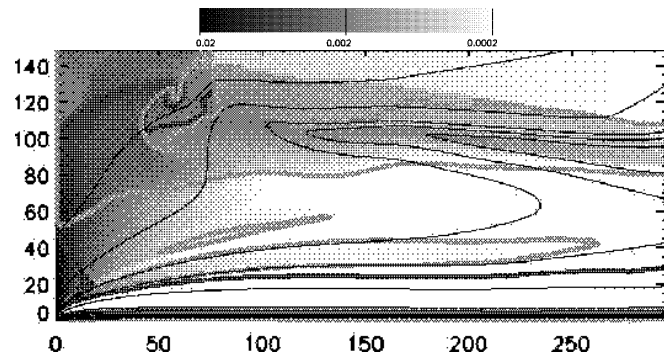


Fig. 11.— Simulation run with different disk boundary conditions (see Tab. 1). Example **i8** ($t = 290$) for a parameter run with the Alfvén surface entering the disk surface. Density and poloidal magnetic field lines. See Fig. 1 for further notation.

REFERENCES

- Bacciotti, F., Ray, T.P., Mundt, R., Eisloffel, J., & Solf, J. 2002, 576, 222
- Blandford, R.D., & Payne, D.G., 1982, MNRAS, 199, 883
- Camenzind, M. 1990, Magnetized disk-winds and the origin of bipolar outflows, in: G. Klare (ed.) *Rev. Mod. Astron.* 3, Springer, Heidelberg, p.234
- Casse, F., & Keppens, R. 2002, ApJ, 581, 988
- Cemeljic, M., & Fendt, C. 2004, Launching of Resistive Magnetic Protostellar Jets, in A.K. Dupree and A.O. Benz (eds) *Stars as suns: activity, evolution and planets*, Proceedings of the 219th IAU symposium 219, Astronomical Society of the Pacific.
- Chiueh T., Li Z.-Y., & Begelman M.C. 1991 ApJ, 377, 462
- Contopoulos, J., & Lovelace, R.V.E. 1994, 429, 139
- Curry, C.T., & McKee, C.F. 2000, ApJ, 528, 734
- Fendt, C., Camenzind, M., & Appl, S. 1995, A&A, 300, 791
- Fendt, C., & Camenzind, M. 1996, A&A, 313, 591
- Fendt, C., & Elstner, D. 1999 A&A, 349, L61
- Fendt, C., & Elstner, D. 2000, A&A, 363, 208
- Fendt, C., & Memola, E. 2001, A&A, 365, 631
- Fendt, C., & Camenzind, M. 2002, A&A, 395, 1045
- Ferreira, J. 1997, A&A, 319, 340
- Gammie, C.F., & Ostriker, E.C., 1996, ApJ, 466, 814
- Hawley, J.F., & Stone J.M. 1995, *Comp. Physics Comm.*, 89, 127
- Hayashi, M.R., Shibata, K., & Matsumoto, R. 1996, ApJ, 468, L37
- Heyvaerts, J., & Norman, C.A. 1989, ApJ, 347, 1055
- Heyvaerts, J., & Norman, C.A. 2003, ApJ, 596, 1256
- Kato, S.X., Kudoh, T., & Shibata, K. 2002, ApJ, 565, 1035

- Kigure, H., & Shibata, K. 2005, astro-ph/0508388
- Krasnopolsky, R., Li, Z.-Y., & Blandford, R. 1999, ApJ, 526, 631
- Kudoh, T., Matsumoto, R., & Shibata, K. 1998, ApJ, 508, 186
- Kudoh, T., Matsumoto, R., & Shibata, K., 2002, PASJ, 54, 267
- Kuwabara, T., Shibata, K., Kudoh, T., & Matsumoto, R. 2000, PASJ, 52, 1109
- Kuwabara, T., Matsumoto, R., & Shibata, K. 2005, PASJ, 54, 121
- Lery, T., Heyvaerts, J., Appl, S., & Norman, C. A. 1998, A&A, 337, 603
- Li, Z.-Y., Chiueh, T., & Begelman, M.C., 1992, ApJ, 394, 459
- Li, Z.-Y. 1993, ApJ, 415, 118
- Li, Z.-Y. 1995, ApJ, 444, 848
- Matt, S., Winglee, R., & Böhm, K.-H. 2003, MNRAS, 345, 660
- McKee, C.F., & Zweibel E.G. 1995, ApJ, 440, 686
- Michel, F.C. 1969, ApJ, 158, 727
- Miller, K.A., & Stone, J.M. 1997, ApJ, 489, 890
- Okamoto I. 2003, MNRAS, 318, 250
- Ouyed, R., & Pudritz, R.E., 1997a, ApJ, 482, 712
- Ouyed, R., & Pudritz, R.E., 1997b, ApJ, 484, 794
- Ouyed, R., & Pudritz, R.E. 1999, MNRAS, 309, 233
- Ouyed, R., Clarke, D., & Pudritz, R.E. 2003, ApJ, 582, 292
- Passot, T., & Vázquez-Semadeni, E. 2003, A&A, 398, 845
- Pudritz, R.E., & Norman, C.A. 1983, ApJ, 274, 677
- Pudritz, R.E., Rogers, C.S., & Ouyed, R. 2006a, MNRAS, 365, 1131
- Pudritz, R.E., Ouyed, R., Fendt, Ch., & Brandenburg, A., Disk Winds, Jets, and Outflows: Theoretical and Computational Foundations, in: B. Reipurth et al. (eds.) Protostars and Planets V, University of Arizona Press, Tucson, 2006b, in press, astro-ph/0603592

- Ramsey, J.P., & Clarke, D.A., Jets from Keplerian Disks and the Role of the Equation of State, poster contr., conference "Cores, Disks, Jets & Outflows in Low & High Mass star forming environments", Banff 2004, see www.ism.ucalgary.ca/meetings/banff/posters.html
- von Rekowski, B., & Brandenburg, A. 2004, *A&A*, 420, 17
- Rüdiger, G., Accretion disk structure with magnetic fields, in: *The Physics of Cataclysmic Variables and Related Objects*, B. T. Gänsicke et al. (eds), ASP Conference Proc., Vol. 261 (2002) p. 317
- Romanova, M.M., Ustyugova, G.V., Koldoba, A.V., & Lovelace, R.V.E. 2002, *ApJ*, 578, 420
- Romanova, M.M., Ustyugova, G.V., Koldoba, A.V., Wick, J.V., & Lovelace, R.V.E. 2003, *ApJ*, 595, 1009
- Romanova, M.M., Ustyugova, G.V., Koldoba, A.V., & Lovelace, R.V.E. 2004, *ApJ*, 616, L151
- Romanova, M.M., Ustyugova, G.V., Koldoba, A.V., & Lovelace, R.V.E. 2005, *ApJ*, 635, L165
- Sauty, C., & Tsinganos, K. 1994, *A&A*, 287, 893
- Sakurai, T. 1985, *A&A*, 152, 121
- Sakurai, T. 1987, *PASJ*, 39, 821
- Spruit H.C., Foglizzo T., & Stehle, R. 1997, *MNRAS*, 288, 333
- Stone, J.M., & Norman, M.L. 1992, *ApJS*, 80, 753
- Stone, J.M., & Norman, M.L. 1992, *ApJS*, 80, 791
- Uchida, Y., & Shibata, K. 1985, *PASJ*, 37, 515
- Ustyugova, G.V., Koldoba, A.V., Romanova, M.M., Chechetkin, V.M., & Lovelace, R.V.E. 1995, *ApJ*, 439, L39
- Ustyugova G.V., Koldoba A.V., & Romanova M.M., Chechetkin V.M., & Lovelace R.V.E. 1999, *ApJ*, 516, 221
- Vitorino, B.F., Jatenco-Pereira, V., & Opher, R. 2003, *ApJ*, 592, 332